the plant journal

SEB SOCIETY FOR EXPERIMENTAL BIOLOGY

The Plant Journal (2023) **116,** 1825–1841 doi: 10.1111/tpj.16456

TECHNICAL ADVANCE

Fluorescence-activated multi-organelle mapping of subcellular plant hormone distribution

Vladimír Skalický[1,†], Ioanna Antoniadi[2,†], Aleš Pěnčík[1], Ivo Chamrád[1], René Lenobel[1], Martin F. Kubeš[1], Marek Zatloukal[3], Asta Žukauskaitė[3], Miroslav Strnad[1], Karin Ljung[2,*] and Ondřej Novák[1,2,*]

[1]*Laboratory of Growth Regulators, Faculty of Science, Palacký University and Institute of Experimental Botany of the Czech Academy of Sciences, CZ-78371 Olomouc, Czech Republic,*

[2]*Umeå Plant Science Centre, Department of Forest Genetics and Plant Physiology, Swedish University of Agricultural Sciences, SE-90183 Umeå, Sweden, and*

[3]*Department of Chemical Biology, Faculty of Science, Palacký University, CZ-78371 Olomouc, Czech Republic*

Received 3 March 2023; revised 17 August 2023; accepted 26 August 2023; published online 8 September 2023.
*For correspondence (e-mail karin.ljung@slu.se; novako@ueb.cas.cz).
†These authors contributed equally to this work.

SUMMARY

Auxins and cytokinins are two major families of phytohormones that control most aspects of plant growth, development and plasticity. Their distribution in plants has been described, but the importance of cell- and subcellular-type specific phytohormone homeostasis remains undefined. Herein, we revealed auxin and cytokinin distribution maps showing their different organelle-specific allocations within the Arabidopsis plant cell. To do so, we have developed Fluorescence-Activated multi-Organelle Sorting (FAmOS), an innovative subcellular fractionation technique based on flow cytometric principles. FAmOS allows the simultaneous sorting of four differently labelled organelles based on their individual light scatter and fluorescence parameters while ensuring hormone metabolic stability. Our data showed different subcellular distribution of auxin and cytokinins, revealing the formation of phytohormone gradients that have been suggested by the subcellular localization of auxin and cytokinin transporters, receptors and metabolic enzymes. Both hormones showed enrichment in vacuoles, while cytokinins were also accumulated in the endoplasmic reticulum.

Keywords: Auxin, cytokinin, *Arabidopsis thaliana*, subcellular homeostasis, subcellular fractionation, flow cytometry, LC–MS/MS, technical advances.

INTRODUCTION

Plant hormones have intertwined homeostatic regulation (Šimášková et al., 2015; Tessi et al., 2021) and control plant growth, development and plasticity (Schaller et al., 2015) by acting synergistically (Hurný et al., 2020) or antagonistically (Müller & Sheen, 2008). Auxin and cytokinin (CK) relevant enzymes' and transporters' localizations indicate hormonal homeostasis control at the subcellular level (Skalický et al., 2018), yet the existence of intracellular distribution gradients of the phytohormones is elusive. Initial steps of auxin and CK biosynthesis occur mainly in chloroplasts (Skalický et al., 2018; Zürcher & Müller, 2016). The active auxin compound, indole-3-acetic acid (IAA), can be produced by parallel biosynthetic pathways and reversibly conjugated with amino acids or glucose (Hayashi et al., 2021). However, the major IAA catabolic pathway in Arabidopsis is oxidation to 2-oxindole-3-acetic acid (oxIAA) (Casanova-Sáez et al., 2021; Hayashi et al., 2021). CK nucleotides are the first synthetized CK forms originating from adenine (Kakimoto, 2001). CK nucleotides can then be converted, either directly to highly active free-bases or indirectly via the production of the intermediate riboside forms (Kurakawa et al., 2007). CK bases can be stored as CK *O*-glucosides (Kiran et al., 2012), inactivated into CK *N*-glucoside forms (Wang et al., 2013), or irreversibly degraded back to adenine by cytokinin oxidase/dehydrogenase (Werner et al., 2006).

Auxin and CK cell-type-specific distribution has been studied within the Arabidopsis root tip (Antoniadi et al., 2015; Pěnčík et al., 2013; Petersson et al., 2009). Studies of phytohormone profiles and different physiological

processes at the subcellular level require compartment isolation in enriched and pure fractions. Conventional organelle isolation by density-gradient (ultra)centrifugation has so far been considered the gold standard (Millar & Taylor, 2017). However, the continuously increasing sensitivity of the downstream instrumental analysis over the last decades demands organelle isolation approaches with higher resolving power. Therefore, advanced affinity-capturing (Deal & Henikoff, 2011; Niehaus et al., 2020) and flow-cytometric methods (Petrovská et al., 2014; Wolf et al., 2005) have been established. As a result, rapid development and improvements in mass-spectrometric methods, as well as sample isolation techniques, have enabled substantial progress in cell-type-specific and subcellular studies over the last decade (Novák et al., 2017).

Herein, we reveal the intracellular distribution of auxin and CKs in nuclei, chloroplasts, mitochondria, endoplasmic reticulum (ER) and vacuoles. To achieve that, we introduced a breakthrough technique, so-called Fluorescence-Activated multi-Organelle Sorting (FAmOS), for the simultaneous fractionation of four organelle populations from a single sample. This time-efficient method is based on flow-cytometric principles, utilizes organelle-specific fluorophores and considers hormone metabolism stability. We combined our recently developed FAmOS tool with ultrasensitive mass spectrometry-based methods. Apart from the four organelles isolated via FAmOS, vacuoles have been collected by density-gradient centrifugation to complete the subcellular hormone map. Altogether, this provides a unique approach for organelle-specific metabolic profiling of auxin and CKs, combined with other "omics" applications such as proteomics and metabolomics. Shedding light on regulatory processes at the subcellular level will allow a deeper understanding of plant developmental processes and cellular homeostasis maintenance, as well as in intra- and intercellular communication.

RESULTS

Multi-organelle fluorescent staining for four-way sorting

Previous studies on metabolic phytohormonal gradients between different cell types relied on differentiated cells within the plant tissues (Antoniadi et al., 2015; Pěnčík et al., 2013; Petersson et al., 2009). Visualized auxin and CK signalling by synthetic sensors (Liao et al., 2015; Zürcher et al., 2013), fluorescently labelled phytohormone analogues (Hayashi et al., 2014; Kubiasová et al., 2020) or mathematical models (Band et al., 2014; Di Mambro et al., 2017) showed also concentration gradients within the plant tissue. To ensure higher level of uniformity, as a biological model for our metabolic profiling at the subcellular level we opted to use an undifferentiated pluripotent cell line of *Arabidopsis thaliana* Col-0 originated from root tissue (Pesquet et al., 2010). Chloroplasts were analysed according to their chlorophyll auto-fluorescence while for analysis of nuclei, ER and mitochondria, organelle-specific fluorescent dyes were employed (Boussardon et al., 2020; Haas et al., 2016; Wolf et al., 2005). These live-staining dyes were carefully selected in order to minimize spectra overlap based on their respective excitation and emission wavelengths. Thus, we could achieve multicolour labelling and distinguish four different organelles deriving from the same cell (Figure 1; Figure S1).

The localization specificity of the selected fluorescent dyes was validated in plant cells. Protoplasts derived from three transgenic plant lines with endogenous expression of green or yellow fluorescent protein (GFP or YFP, respectively) in ER, mitochondria and nuclei, (Boisnard-Lorig et al., 2001; Logan & Leaver, 2000; Matsushima et al., 2002), were stained with the corresponding fluorescent dye. As shown in Figure 1a, the endogenous fluorescence of each transgenic plant line co-localized with the applied dye-emitted fluorescence for the respective compartment. Finally, imaging of wild-type protoplasts stained with the mixture of the ER-tracker, MitoTracker and Hoechst dyes, labelling ER, mitochondria and nuclei, respectively, confirmed the specific labelling of each fluorescent dye within the cell and demonstrated the absence of labelling artefacts or doubly stained organelles (Figure 1b).

Simultaneous sorting of four organelle populations

Identification of distinct organelle populations during FAmOS required their measured optical characteristics, including relevant size, granularity, complexity and specific fluorescence. According to these analysed parameters, we developed a sequential (three-step) gating strategy (Figure S2), leading to the classification and selection of four distinct organelle populations as representatively shown in Figure 1c.

The first step of our gating strategy was excluding debris and aggregates, which did not fit in the relevant organelle diameter size range of 2–10 μm (Figure S2a). The second step was the absolute identification of particular organelle populations, based on their characteristic fluorophore signal. This specific signal for each organelle population individually, had been defined in advance using appropriate negative control samples (Figure S2b). During this second step, a sequential exclusion strategy was incorporated according to the abundance and brightness of each fluorescent organelle. Since the identified chloroplast population accounted for nearly 20% of all measured particles, they were selected as the first population to gate. They were thus further excluded from the subsequent organelle populations' identification process. Following the same principle, the gate design was sequentially continued for nuclei, ER and finally mitochondria, as shown in Figure S2b. The third and final step of our gating strategy was the distinction between droplets containing a single

organelle and more than one organelle (Figure S2a). To achieve this, we analysed the ratio of each fluorescence signal width to the respective area (Suda et al., 2007). The designed gates finally allowed sufficient organelle separation and efficient simultaneous sorting of mitochondria, nuclei, ER and chloroplast populations in four individual vials. Representative output of the four organelle populations is shown in Figure 1c.

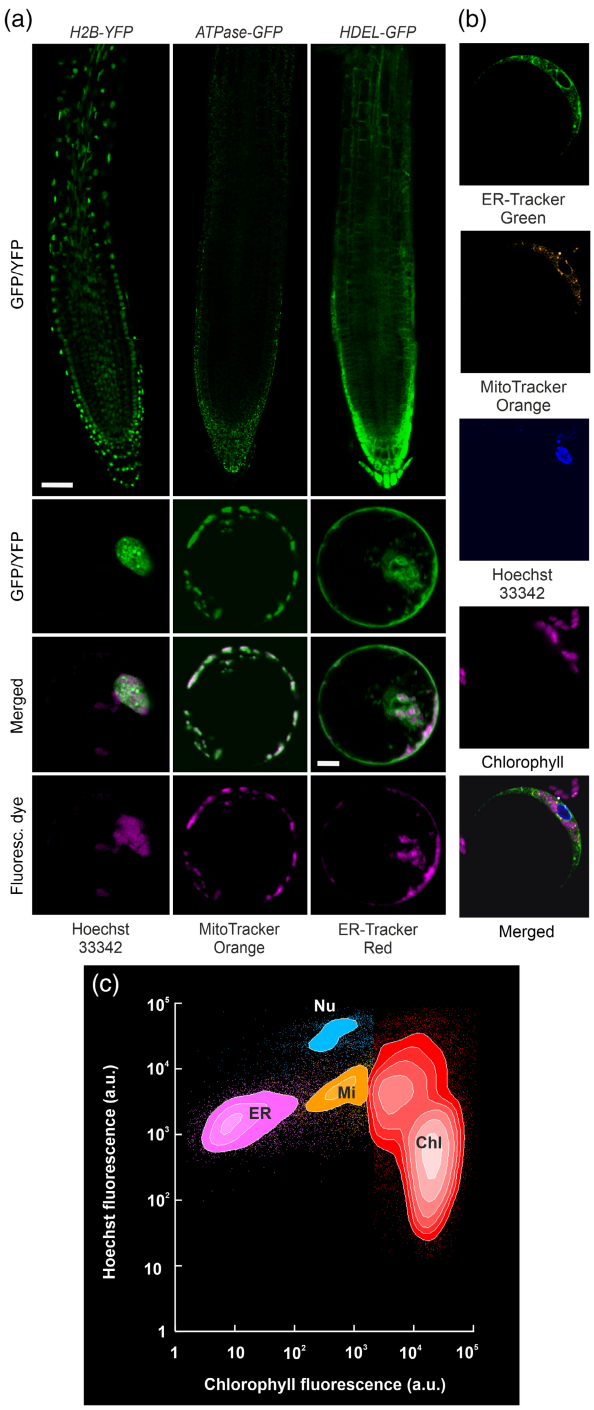

Figure 1. Selection of fluorescent dyes and verification of their specificity.
(a) Co-localisation of the fluorescence of the organelle marker lines *HISTONE 2B:YFP (H2B-YFP), β-ATPase subunit:GFP* (*ATPase-GFP) and HDEL: GFP* and the respective fluorescent dyes Hoechst 33342, MitoTracker Orange and ER-Tracker Green (left to right as indicated). Images of root tips show fluorescent line expression. Protoplast suspensions were prepared from these lines and stained with the respective fluorescent dye.
(b) Protoplasts derived from 14-day-old light cell culture stained with the pool of three fluorescent dyes (ER-Tracker Green (green), MitoTracker Orange (orange) and Hoechst 33342 (blue)). Chloroplasts are shown in purple.
(c) Final representative separation of organelle population by FAmOS after their identification. Scale bars in root and protoplast pictures are 40 and 5 μm, respectively. Chl – Chloroplasts, ER – endoplasmic reticulum, Mi – mitochondria, Nu – nuclei.

Identity confirmation of the sorted organelle populations

After completing the gate design (Figure S2a), we performed several tests to confirm the identity of the FAmOS-sorted organelle populations (Figure S3). The identity of enriched organelle fractions was initially assessed by determining the presence of protein markers by immunoblot analysis (Včelařová et al., 2021). While the results confirmed substantial enrichment in chloroplast and nuclear fractions, no antibody signal was detected in either the ER or the mitochondrial fraction (Figure S3a). This could be due to the combination of nanogram protein input and the limited sensitivity of the antibodies used for immunoblotting.

To overcome this issue, we performed a qualitative evaluation of proteins present in the isolated organelle fractions by proteomic analysis and functional annotation clustering of statistically enriched gene ontology (GO) terms (Huang et al., 2009). Altogether, 401 Arabidopsis proteins were unambiguously identified in the samples (Figure 2a). Approximately 28% of these proteins were common for at least three sorted fractions, presumably originating from the cytoplasm and/or sharing multiple cellular localizations (Lee et al., 2010). Notably, cellular processes essential for each sorted organelle population were found among five of the most enriched GO clusters (Figure 2b,c). These annotation groups were observed despite the presence of the above-mentioned common proteins, which generally constitute even more than 80% of the total protein content of the photosynthetically active plant tissues (Niehaus et al., 2020) and easily enshroud signals of less abundant proteins (Huber et al., 2003). Furthermore, several well-known organelle marker proteins such as H3 and inner nuclear membrane protein SUN domain-containing protein 2 (SUN2), reticular chaperone luminal-binding protein 2 (BIP2), or mitochondrial outer membrane protein porin 3 (VDAC3) were found in the expected organelle fractions. Hence, the combination of the GO terms and the specific marker proteins identified in each sorted fragment highlights the specific sorting ability of the developed FAmOS method.

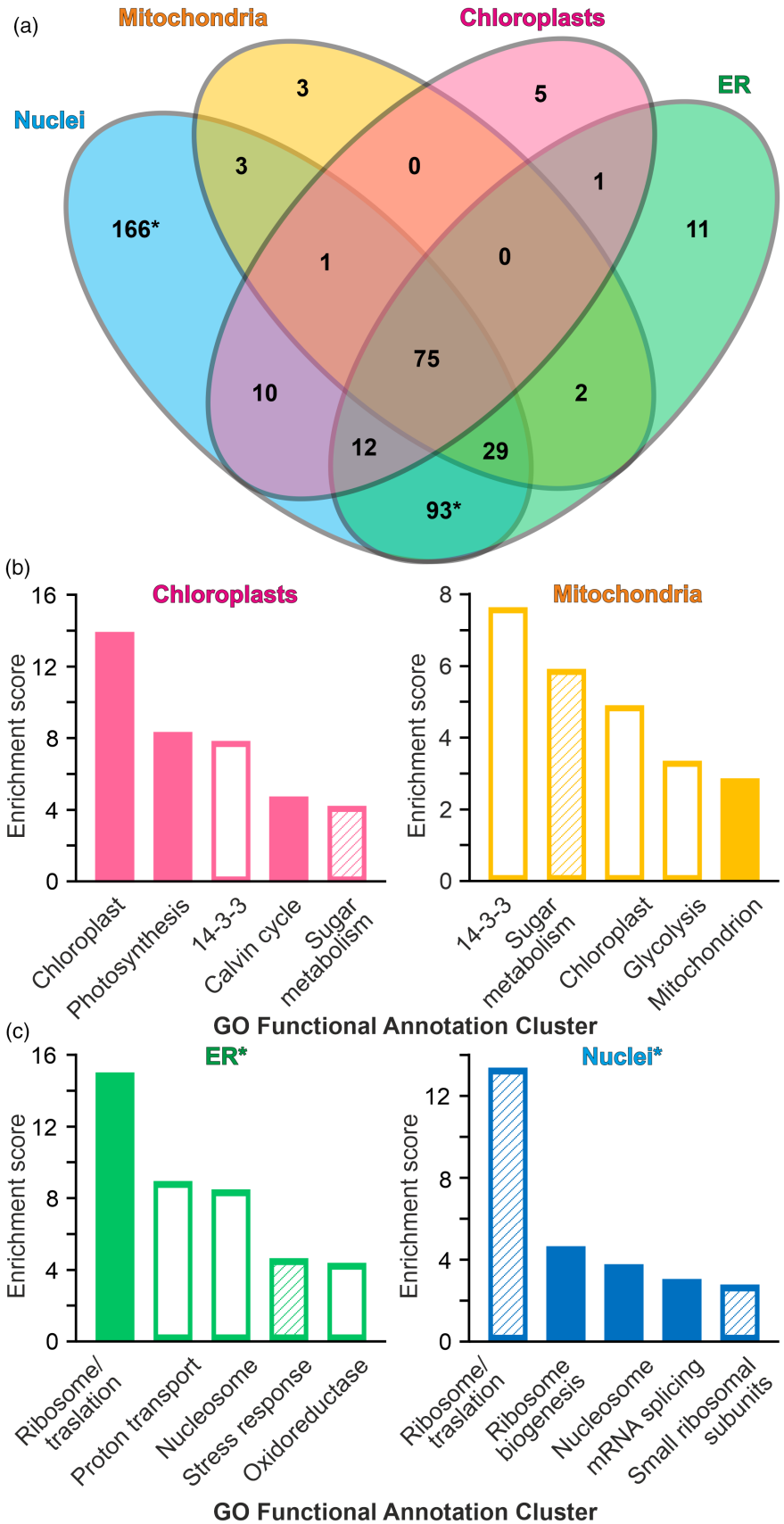

Figure 2. Confirmation of the sorted organelle populations by proteomic analysis.
(a) Venn diagram showing protein identification overlaps for the sorted organelle populations. Numbers represent the total sums of identifications belonging to the corresponding cross-section of the diagram. Asterisk indicates the set of proteins used for the gene ontology (GO) analysis in panel c.
(b,c) Clustering of statistically enriched functional annotation GO terms for proteins identified in particular organelle fraction. Bars depict annotation clusters. The name of the cluster correlates with the individual annotation term with the lowest enrichment *P*-value. The clusters are arranged according to their enrichment score, which is a minus log transformation of the geometric mean of all the enrichment *P*-values of all annotation terms in the given cluster. The bar colours correspond to the respective fraction presented in panel a. Coloured bar indicates a strong functional relationship between the annotation cluster and the respective organelle. Striped bars stand for loose relations. White bars indicate no obvious or too general functional relations.

Phytohormone profiles are stable during FAmOS

We performed a series of control experiments to evaluate the FAmOS influence on auxin and CK metabolisms (Schematic representation in Figure S4). At first, we showed that CK and auxin concentrations remained unaffected in stained organelle suspension compared to the unstained sample, confirming that the fluorescent dye pool used had no impact on the phytohormone levels (Figure S5a). Then, we imitated the sorting process by incubating the organelle suspension in a sorting buffer at 4°C. Subsequent assessment of phytohormone profile stability in several time points revealed no significant alteration of auxin metabolism (Figure 3a) nor conversion between different CK types (Figure 3b). However, the levels of CK precursors, nucleotides and ribosides increased after the organelle suspension was incubated for 2 h at 4°C (Figure 3a). To overcome this problem, we assessed the possibility of halting metabolic processes by performing chemical treatments (Figure S5b–f).

Initially, we attempted mild fixation with formaldehyde to stop all metabolic processes (Petrovská et al., 2014). However, this step was excluded as formaldehyde was detrimental to detecting phytohormones by LC–MS/MS (Skalický et al., 2021) (Figure S5b). Next, we applied sodium azide as an ATP-dependent processes inhibitor (Tucker, 1993) or 1-*N*-naphtylphthalamic acid (NPA) as auxin transport inhibitor (Petrášek et al., 2006). Both had no significant influence on CK and auxin metabolic profiles in organelle suspension (Figure S5c,d). Parallel treatments with adenosine 5′-monophosphate as substrate competitor of phosphatases, or with adenine as CK transport antagonist (Cedzich et al., 2008), further enhanced CK nucleotides or CK ribosides deviation from endogenous levels (Figure S5e,f). Finally, we mixed commonly used phosphatase inhibitors (Breitkopf et al., 2010), which proved to be effective treatment for blocking CK precursors' accumulation during sorting imitation process (Figure 3c). To further diminish potential effects on the hormone metabolism during sample preparation steps, we also shortened our sample incubation time to the minimum by preparing fresh samples every half an hour (Figure S4a).

The final overview on phytohormone profile stability during the whole FAmOS procedure, from sample homogenization to sorting, was achieved by monitoring their metabolism based on fluxomic principles using *in vivo* labelling (Xu et al., 2020). We spiked the organelle suspension sample with stable-isotope labelled standards of active auxin and CK, [$^{13}C_6$]IAA and [$^{15}N_4$]isopentenyladenine ([$^{15}N_4$]iP), respectively, and collected 200 000 organelles per organelle population using FAmOS. The labelled-hormone quantification took place in the pool of the isolated organelles to determine a representative distribution of isotopic labels in all sorted organelle populations. Our findings revealed a 1.8% and 0.8% conversion of [$^{13}C_6$]IAA and [$^{15}N_4$]iP during sorting, respectively (Figure 3d). Moreover, as presented in Figure S5g, we identified a negligible metabolic turnover of 2.1% and 0.2% for the isotopically labelled IAA and iP, respectively, during sample preparation. Altogether, the metabolic turnover of labelled IAA and iP during FAmOS did not exceed 4% and 1%, respectively, suggesting that the phytohormone profiles measured downstream of the developed method represent endogenous profiles of auxin and CK metabolites.

Subcellular phytohormone maps

With FAmOS development, we achieved simultaneous sorting of four intracellular compartments that have undergone identical isolation procedures. We quantified endogenous auxin and CK metabolite levels in 200 000 organelles of each population deriving from the organelle suspension prepared from the cell culture aliquot. To obtain an overall picture of the distribution of phytohormones at the subcellular level, we also performed the analysis in vacuoles isolated by Ficoll density gradient centrifugation from another aliquot of cell culture as described previously (Robert et al., 2007). It was not possible to include vacuole sorting in the FAmOS-collected samples due to their high fragility and size. To maintain their membrane integrity mannitol would need to be added to the organelle suspension solution. However, mannitol often interfered with the resolution of the FACS instrument as it was creating a background of events during cytometric analysis. In addition, including vacuoles in FAmOS would result in significantly increased time of the experimental procedure and this factor, as shown in Figure 3a, can be critical for hormone metabolism. The time would increase both due to the longer isolation process that vacuoles require and to longer sorting time. While auxin and/or CK levels have been previously measured in chloroplasts (Polanská et al., 2007), vacuoles (Jiskrová et al., 2016; Ranocha et al., 2013), ER (Včelařová et al., 2021) and nuclei (Skalický et al., 2021), sample preparation processes and the divergent normalization methods

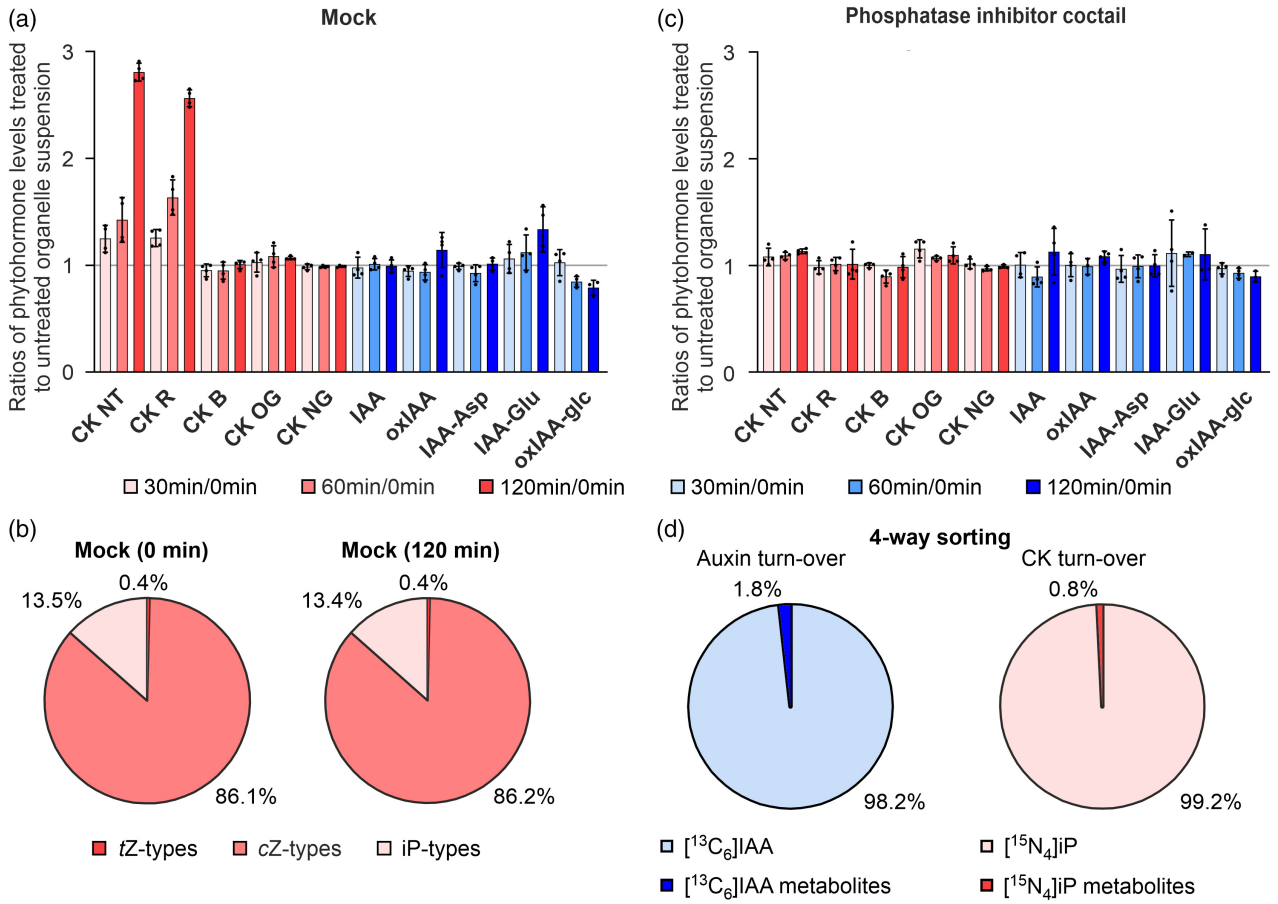

Figure 3. Evaluation of phytohormone profile stability.
(a,c) Stability of cytokinin and auxin profiles in organelle suspension treated without (a, Mock) or with phosphatase inhibitor cocktail (c) and left on ice during the simulated sorting procedure for up to 120 min. The endogenous concentrations of auxins and cytokinins were calculated as pmol per 1 000 000 cells. The results are expressed as the respective ratios of metabolite concentration at time point to metabolite concentration at 0 min (Mean ± SD, $n = 4$). IAA-glucosyl ester was not detected.
(b) Monitoring changes in the distribution of CK types (*tZ, trans*-zeatin; *cZ*, *cis*-zeatin; and iP, isopentenyladenine) in the organelle suspension after a 2h incubation at 4°C. Metabolite profiles are expressed in percentages showing the relative abundance of each CK type ($n = 4$).
(d) Metabolic turnover of isotopically labelled [$^{13}C_6$]IAA and [$^{15}N_4$]iP during 30-min of the four-way sorting process. The complete profile of cytokinin and auxin metabolites labelled with the appropriate stable isotope was determined by LC-MS/MS. Their concentration was calculated as pmol/1 000 000 sorted organelles and is shown as the relative distribution of the respective stable isotope in the cytokinin and auxin metabolites. IAA – indole-3-acetic acid, oxIAA – 2-oxindole-3-acetic acid, IAA-Asp – IAA-aspartate, IAA-Glu – IAA-glutamate, oxIAA-glc – oxIAA-glucosyl ester, NT – CK nucleotides, R – CK ribosides, B – CK free bases, OG – CK *O*-glucosides and NG – CK *N*-glucosides.

used did not allow comparison of the data between the organelles. Due to the different sizes, shapes and abundance of organelles per plant cell, data normalization was essential for comparison of auxin and CK levels between organelles. Phytohormone levels in chloroplasts are usually normalized per chlorophyll content (Polanská et al., 2007), however, this manner of recalculation cannot be applied to other organelles. An accurate normalization method would probably require determination of the volume of the organelles. However, organelle size and volume depend on cell-type and/or organ origin (Pavlova et al., 2021) and estimation of ER volume is highly challenging. Therefore, the data normalization process used here was based on the protein content of the organelle fraction (Včelařová et al., 2021). Protein and phytohormone content in particular fractions were calculated per 10^6 organelles (Tables S1 and S2). The phytohormone concentrations were then determined as pmol/μg of proteins, and the respective subcellular maps of auxin and CK were finally expressed as the ratio of compound(s) levels in each organelle to compound(s) levels in chloroplasts.

Overall, the quantification of 14 endogenous hormonal metabolites was accomplished in five organelle fractions using ultra-sensitive LC–MS/MS. In the organelle suspension sample (prior sorting), auxin metabolites were unambiguously detected, except IAA-glucosyl ester (IAA-glc; Figure 3a). In agreement, IAA-glc was also below the detection limit of in Arabidopsis cell culture

(Table S3). The generated auxin subcellular map, exhibited in Figure 4, concerns metabolites distribution in mitochondria, ER, nucleus, chloroplasts and vacuoles and revealed an auxin gradient with maxima in vacuoles. Undoubtedly, the occurrence of IAA and its metabolites cannot be excluded from cytosol nor other non-analysed organelles (e.g. Golgi apparatus and peroxisomes), which might also be another important pool of phytohormones. Interestingly, oxidized forms of IAA showed a similar pattern to free IAA (Figure 4b). In comparison, amino acid-conjugated auxins (IAA-aspartate and IAA-glutamate) were detected exclusively in vacuoles, while they were below the limit of detection in other analysed compartments (Table S4). The amount of IAA-Asp in vacuoles exceeded the IAA levels (Table S2). However, when whole cells were analysed, IAA surpassed IAA-Asp by 7.6-fold (Table S3). These results are in agreement with the auxin levels reported in previous work (Novák et al., 2012), where the IAA content in roots was at least 10 times higher than that of IAA-Asp.

The most abundant CKs in the organelle suspension sample were *cis*-zeatin-types (*c*Z), accounting for 88% of the total CKs detected (Figure 3b). The iP-types were only present at 12%, while the levels of *trans*-zeatin-CKs (*t*Z) were close to the detection limit of the LC-MS/MS method. The proportion of CK types within organelle suspension corresponds to distribution within the cell culture used in this study (Figure S5h). The intracellular map of CK pool uncovered by FAmOS revealed the hormone's gradient with maxima pivotally in the vacuole and secondarily in the ER (Figure 4a). This subcellular distribution was supported for all isoprenoid CK groups, except from *t*Z-types (Figure S6). Interestingly, exclusive detection of CK *O*-glucosides in the vacuolar fraction (Table S4) is in accordance with the hypothesis that CK storage forms are located in this compartment (Sakakibara, 2006). In contrast, CK nucleotides were below the detection limit in this compartment (Figure 4c) which corresponds with the respective enzymatic localization of ISOPENTENYLTRANSFERASEs (IPTs) (Kasahara et al., 2004). These enzymes, are responsible for the biosynthesis of CK nucleotides and occur mainly in chloroplasts (Skalický et al., 2018) where CK nucleotide gradient maxima were observed (Figure 4c). The active compounds, CK bases, were also found abundantly in chloroplasts compared to mitochondria, ER and nuclei populations.

Our results indicate that in both cases of auxin and CK metabolisms, vacuoles play an essential role as a storage compartment (Figure 4). That is because all detected phytohormone forms accumulated in this compartment or are even exclusively present there.

Monitoring of phytohormone metabolism within the cell

To confirm our results, we also performed FAmOS on aliquots of cell culture that have been incubated with [$^{13}C_6$]IAA and [$^{15}N_4$]iP (Figure 5a,b; Table S5). Both subcellular maps showed dynamic changes in hormonal metabolism at the cell level. Stable-isotope labelled [$^{13}C_6$]IAA confirmed the identified auxin gradient within the cell and the rapid inactivation of IAA by conjugation and oxidation. Interestingly, our findings showed no [$^{13}C_6$]IAA enrichment in any isolated organelle fraction after 2 h-incubation. Moreover, all labelled IAA metabolites were mainly enriched in the vacuole and ER (Figure 5a). The increased oxIAA-glucosyl ester (oxIAA-glc), the most abundant auxin metabolite in Arabidopsis (Pěnčík et al., 2018), was detected in nuclei and mitochondria. High levels of labelled IAA-aspartate and IAA-glutamate following the IAA treatment, probably corresponded to a rapid response of GH3 to the excess of active auxin (Mellor et al., 2016). Similarly, our findings regarding the CK subcellular gradient were further supported by a feeding experiment using labelled [$^{15}N_4$]iP (Figure 5b). Surprisingly, labelled iP was found enriched not only in the vacuole and ER but also in mitochondria. This active CK form converted to ribosides and nucleotides was also found enriched in the vacuole and ER. After 2 h of the feeding experiment, iP seemed to be mainly inactivated, as the respective irreversibly conjugated *N*-glucosides, being the most abundant labelled form accumulated in vacuoles (Figure 5b; Table S5).

DISCUSSION

Previously introduced subcellular fractionation strategies or organelle isolation procedures have been based on distinct principles e.g., sedimentation velocity, density, electrophoretic mobility or immunoaffinity purification (reviewed in Lee et al., 2010) and most of them concerned only one type of organelle. Flow cytometry has been earlier used for cell sorting in human medicine (Adan et al., 2017) as well as in plant sciences (Carter et al., 2013; Galbraith et al., 2021). This technique has been also utilized for sorting of nuclei (Petrovská et al., 2014; Skalický et al., 2021), chloroplasts (Wolf et al., 2005) or even smaller particles like chromosomes (Thind et al., 2017). Here we used the FACS instrument and achieved a 4-way simultaneous and efficient sorting of chloroplasts, nuclei, ER and mitochondria from a single sample. An advantageous aspect in FAmOS is that organelle sorting can be live-monitored, documented and in parallel analysed by several parameters. For example, the data generated during FAmOS include the number of particles that passed in front of the laser, their relative size and granularity/complexity and their (auto)fluorescent signal intensities. These values can be used for further calculations (organelle yield) or normalized data projection (number of organelles sorted). In addition, our FAmOS method development was designed for versatile use, in terms of sample preparation and downstream application possibilities. This additionally empowers FAmOS as a compelling tool for various different subcellular studies.

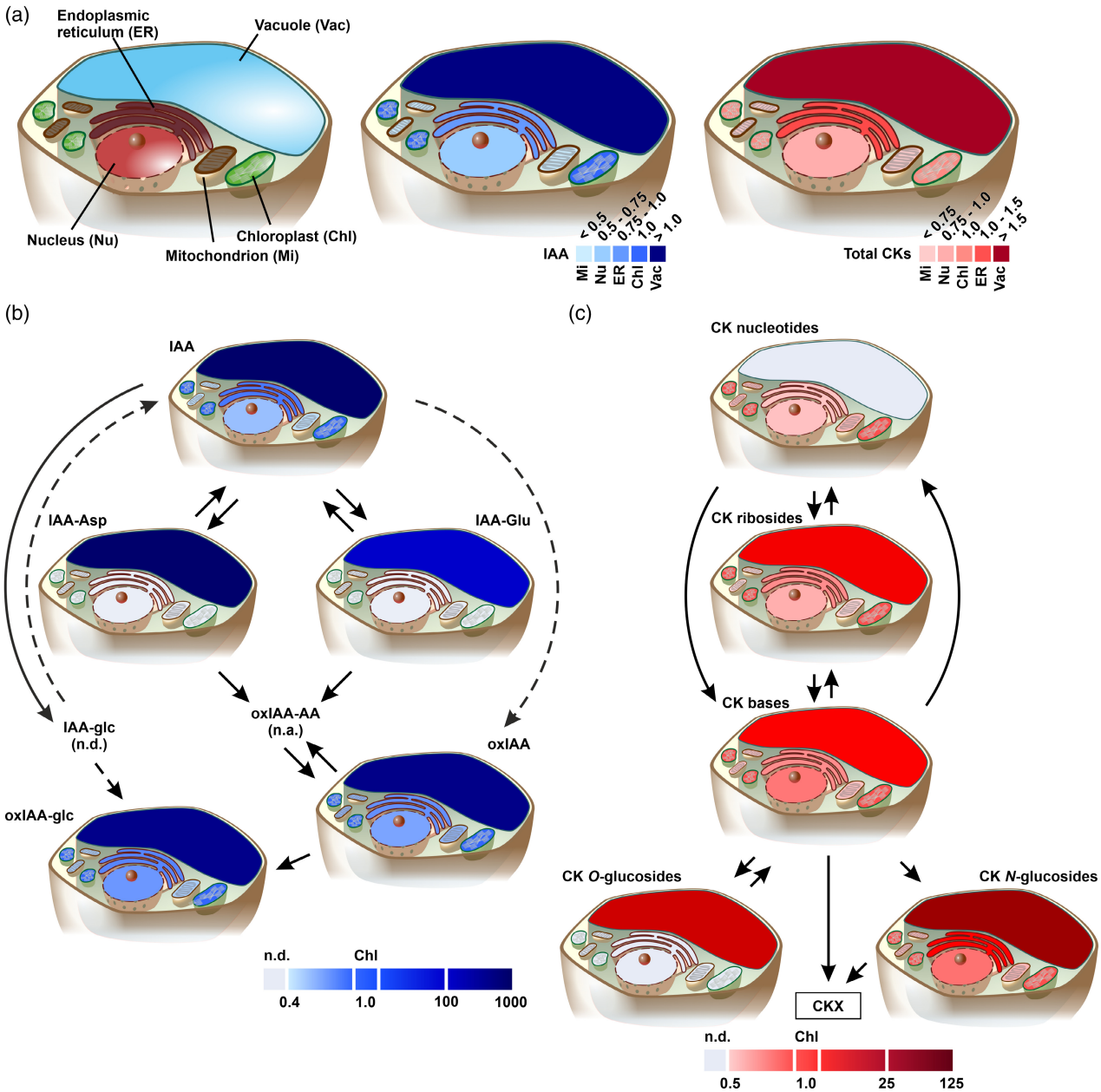

Figure 4. Subcellular map of endogenous phytohormones within the Arabidopsis cell.
(a) Scheme of a plant cell (left), relative distribution of auxin (middle in blue) and total cytokinin metabolites (right in red) within the plant cell.
(b) Abundance of IAA metabolites (IAA – indole-3-acetic acid, IAA-Asp – IAA-aspartate, IAA-Glu – IAA-glutamate, oxIAA – 2-oxoindole-3-acetic acid, oxIAA-glc – oxIAA-glucosyl ester) within the Arabidopsis cell. IAA-amide conjugates were present only in vacuoles. No IAA-glucosyl ester (IAA-glc) was detected in all organelle-enriched fractions.
(c) Subcellular map of cytokinin metabolite groups (CK nucleotides, ribosides, bases, *O*-glucosides and *N*-glucosides) presents CK metabolism in organelle fractions isolated from Arabidopsis cell cultures. CK *O*-glucosides were not detected in all isolated organelles except vacuoles. The opposite pattern was determined for CK nucleotides not found in vacuoles. The results represent 5 biological replicates. The metabolites were quantified in pmol/μg of proteins, and the ratios of the respective organelle to chloroplast were determined. To estimate the ratio of vacuolar IAA-amino acid conjugates and CK O-glucosides in comparison with their levels in chloroplasts, 2/3 of the detection limit normalized per protein amount for each compound was used. CKX – cytokinin oxidase/dehydrogenase, Chl – chloroplast, n.a. – not analysed, n.d. – not detected.

Initially, live-staining fluorescent dyes were carefully selected according to their spectral properties (Figure S1a) for the identification of the desired organelle populations (Figure 1c). These dyes have been primarily designed in mammalian cells and therefore their subcellular localization specificity was verified in plant cells (Figure 1a,b). The labelling approach chosen facilitates both a rapid multi-staining strategy and bypass of time-consuming

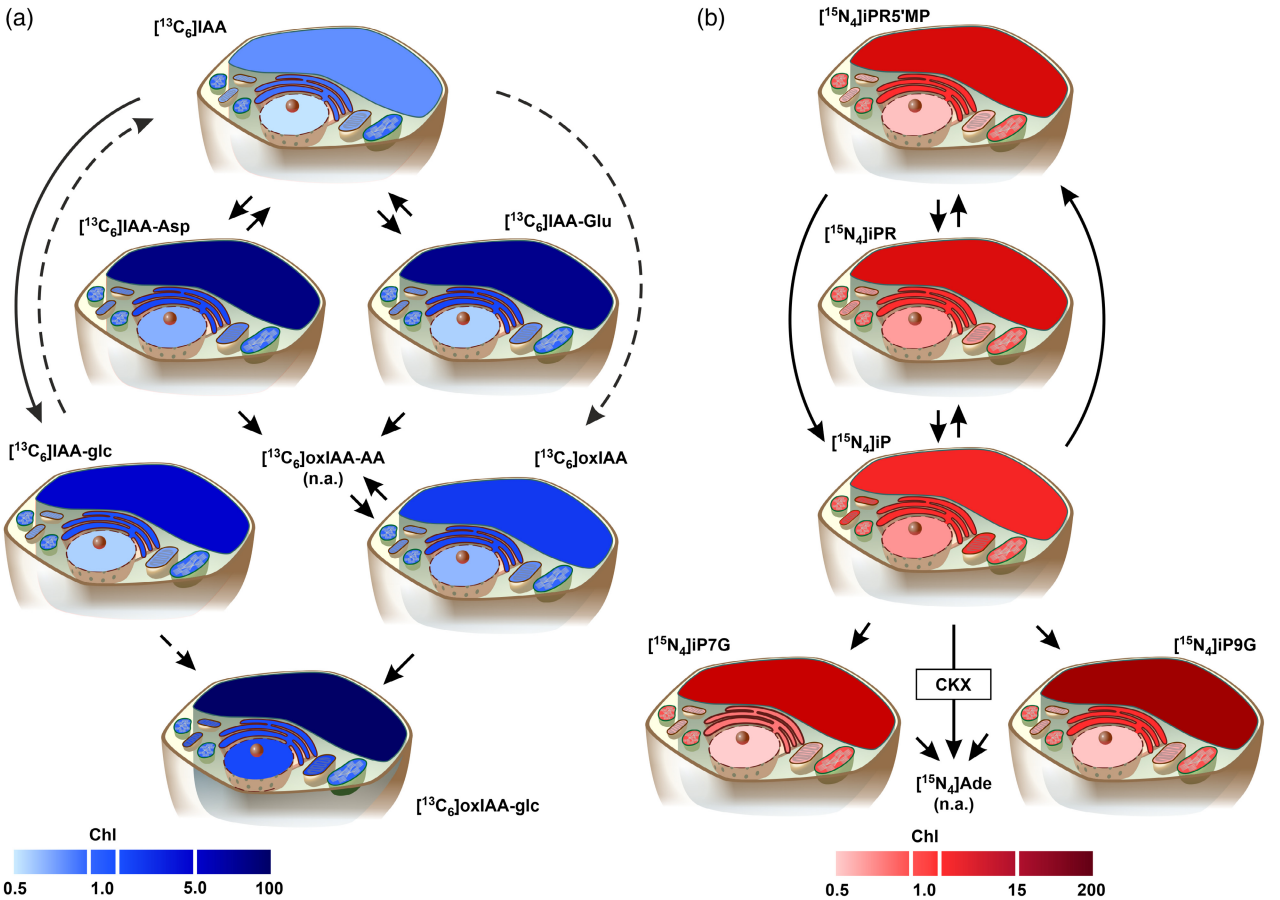

Figure 5. Metabolism of stable-isotope labelled compounds in organelle fractions isolated from Arabidopsis cell cultures.
The suspension culture was treated with 10 μM [$^{13}C_6$]IAA (a, blue) and [$^{15}N_4$]iP (b, red) for 2 h before four-way sorting and vacuole isolation. The enrichment of analytes is expressed as colour scales indicating the phytohormone content as a relative ratio of the absolute level of each metabolite (pmol/μg of proteins) in the organelle fraction to that in the chloroplasts. Five biological replicates were analysed for each organelle type, and for each replicate, at least 200 000 organelles were used. Indole-3-acetic acid (IAA), IAA-aspartate (IAA-Asp), IAA-glutamate (IAA-Glu), IAA-glucosyl ester (IAA-glc), 2-oxoindole-3-acetic acid (oxIAA), oxIAA-glucosyl ester (oxIAA-glc), isopentenyladenine (iP), isopentenyladenosine (iPR), isopentenyladenosine-5′-monophosphate (iPR5′MP), isopentenyladenine-7-glucoside (iP7G), isopentenyladenine-9-glucoside (iP9G), CKX – cytokinin oxidase/dehydrogenase, n.a. – not analysed.

generation and establishment of transgenic fluorescent lines which are often used in methods based on affinity purification (Niehaus et al., 2020). Moreover, the fluorescent dyes can be efficiently applied to various mutant and overexpressing plant lines and thus promote research for the functional relevance of organelles.

Following the live-staining and optimisation of the FACS gates and parameters (Figure 1c; Figures S1 and S2), the selected plant organelles were simultaneously collected into four separate tubes. The identity of the sorted organelle populations was verified in a series of independent experiments comprising immunoblotting (Figure S3a) and LC–MS/MS-based-proteomic protein identification (Figure 2). The latter showed that specific functions could be associated with the respective sorted organelle fraction by GO functional annotation clustering (Huang et al., 2009). Altogether, it can be concluded that the developed FAmOS method empowers simultaneous and sufficient enrichment of chloroplasts, nuclei, ER and mitochondria populations.

To understand how FAmOS process can possibly affect hormone profiles, we performed a series of control experiments. Imitation of the sorting procedure resulted in negligible changes in auxin profile but sharp rise of CK precursors (Figure 3a). Conventional CK extraction from plant tissues employs an acidified organic solvent (Hoyerová et al., 2006). This facilitates enzymatic inactivity and thus stabilised CK metabolome. Unfortunately, such solvent is not compatible with FAmOS due to phospholipid membrane dissolution and protein precipitation. Instead, we examined the possibility of halting all metabolic processes by performing mild tissue fixation with formaldehyde. This treatment conserves organelles and thus results in improved sorting procedure (Levi et al., 1986) as well as in inactivation of all metabolic processes (Petrovská et al., 2014). However, the applied formaldehyde

fixation resulted in phytohormone analysis deterioration (Figure S5b) as was similarly found in Skalický et al. (2021). Possible explanation might be cross-linking of some analytes especially IAA and CK ribosides with cellular structures (Friml et al., 2003). Moreover, the use of different chemical treatments, inspired by two studies dealing with auxin and CK profiling in sorted plant protoplasts (Antoniadi et al., 2015; Petersson et al., 2009), also negatively influenced CK precursor levels (Figure S5). Finally, CK metabolism was stabilised during sorting imitation process after including a mix of phosphatase inhibitors in the sample (Figure 3c). Furthermore, monitoring of isotopically labelled IAA and iP during sorting procedure showed a negligible metabolic turn-over (Figure 3d; Figure S5g). These results indicate that determination of phytohormonal subcellular profile is minimally burdened by artificial changes during FAmOS workflow.

The combination of our innovative developed sorting tool with ultra-sensitive mass spectrometry-based analytical methods enabled a high-resolution mapping of phytohormone metabolites in isolated organelles. However, this challenging task introduced issues such as data normalization between different organelle populations due to their various sizes, volumes, shapes and abundances within the plant cell. In order to emphasize trends and enrichment of individual phytohormones, we chose to normalize the level of phytohormones per protein as a common parameter of all organelles. Although the proteomic results showed a complex matrix background in all our samples (Figure 2), it was not possible to collect blank samples and subtract the background levels. We therefore decided to show ratio of phytohormone levels in particular organelle to chloroplasts, which were the most easily distinguishable, stable and abundant organelle populations during all sorting experiments.

This mapping ultimately makes it possible to better understand signalling, transport and metabolism of plant hormones at the cellular and subcellular levels. Auxin and CK homeostasis maintenance is a strictly regulated coordination of biosynthesis, metabolism, catabolism and transport. Although many aspects of this fine balance have been described during the last two decades (Schaller et al., 2015), its overview within the unit of one cell, yet remains elusive.

For proof-of-concept of the FAmOS methodology, we expressed the intracellular phytohormone gradient maps for auxin and CKs (Figure 4). The concentration gradients revealed within the cell supported our hypothesis that phytohormone distribution is in good agreement with relevant enzymes' and transporters' localizations (Skalický et al., 2018). Our results indicate that in both cases of auxin and CK metabolism, vacuoles play important role potentially as a storage compartment (Figure 4b,c). That is due to all detected phytohormone forms were mainly or even exclusively accumulated there. This could also be explained by the fact that vacuoles may occupy majority of matured plant cell volume.

Hormonomic screening showed 14 endogenous phytohormonal metabolites. As mentioned above, all auxin-related compounds were enriched in vacuoles. IAA levels are considerably regulated by GRETCHEN HAGEN 3 (GH3) enzymes catalysing IAA and amino acid conjugation (Hayashi et al., 2021). However, their localization is not fully known. One of the members, GH3.17, is mainly present in cytosol (Di Mambro et al., 2019). On the other hand, IAA-amino acid conjugates were detected solely in vacuoles. IAA-amino acid conjugate enrichment suggests their possible transport into vacuoles. Interestingly, Ranocha et al. (2013) could not find IAA-Asp in vacuoles, whereas our data showed that its levels exceeded that of IAA itself. In the same study (Ranocha et al., 2013), IAA-glc was the most abundant IAA metabolite in vacuoles but it was not detected in these organelles according to our data. Although it is interesting to present relevant data from other studies, a respective comparison cannot be conclusive because the starting material used for the analysis in Ranocha et al. (2013) is different from our root-derived cell culture in FAmOS. Also, the levels of auxin metabolites are expressed in different units compared to the current study. Similarly, previous work has shown that IAA-glc is highly abundant compound in Arabidopsis roots (Porco et al., 2016), however according to our results it was not detected in any of the organelles tested. This could be due to differences in hormone metabolites in plant tissue where cells are organised, have designated cell identities and "communicating" through active or passive compound transport between them. OxIAA-glc is yet another abundant IAA metabolite in Arabidopsis, usually reported to the present in ng/mg amounts (Porco et al., 2016), although we detected much lower levels. In Table S3, we show that IAA-glc and oxIAA-glc were below the limit of detection at all in examined Arabidopsis cell culture. Similarly, the presence of IAA-glc and oxIAA-glc metabolites in Arabidopsis ecotype Landsberg *erecta* cell culture has not been proven (Skalický et al., 2021). At this point, it should be noted that although we showed that IAA-amino acid conjugates were present only in vacuoles, their presence cannot be excluded from other organelles as these were not truly absent but just below the limit of detection, and this is the case for all compounds. This might be expected though because IAA-Asp is not an abundant compound in Arabidopsis (Hayashi et al., 2021; Novák et al., 2012). Nevertheless, IAA-Asp and IAA-Glu were detected in ER fractions previously (Včelařová et al., 2021). In addition, the hormonal gradients of endogenous IAA and isotopically labelled IAA uncovered by FAmOS were also observed between ER and nuclei (Figures 4a and 5a) as a site of canonical signalling (Cancé et al., 2022), supporting the hypothesis of a putative but unknown molecular player(s) facilitating IAA transport between the ER and the nucleus (Middleton et al., 2018). Importantly, a comparison of our results shown in Tables S2

and S3 predicts that most of the IAA present in the cell could be at a high concentration in the cytoplasm. In the future, the FAmOS technique combined with other biochemical isolation procedures will have the potential to reveal the distribution of phytohormones not only in various organelles but also in the cytoplasm.

Furthermore, CK bases as the active form, were enriched in chloroplasts in comparison with mitochondria, ER and nuclei. In general, CKs promote chloroplast development, moreover, CKs regulate gene transcription and promote proteosynthesis in chloroplasts (Brenner et al., 2012). CK *O*-glucosides were exclusively detected in vacuoles in accordance with the hypothesis that CK storage forms locate to this compartment (Šmehilová et al., 2016). Moreover, Kiran et al. (2012) showed the accumulation of *O*-glucosides in vacuoles by translocation of β-glucosidase to this compartment.

Monitoring of active phytohormones and their related compounds within organelles can lead to revealing of their fate and mechanism of intracellular homeostasis maintenance. *In vivo* labelling was used for monitoring of phytohormonal metabolic pattern, therefore, stable-isotope labelled [$^{15}N_4$]iP and [$^{13}C_6$]IAA were utilized in feeding experiments (Figure 5a,b; Table S5). High levels of isotopically labelled CK glucosides confirmed CK glycosylation as the main inactivation route (Hošek et al., 2020). Unfortunately, adenine, the main product of CK degradation via cytokinin oxidase/dehydrogenase, was not analysed in the same samples due to limitations of the analytical method. Increased levels of labelled iP in ER fraction are coincided with the presence of CK transport facilitator AZA-GUANINE RESISTANT 2 (AZG2) (Tessi et al., 2021) together with CK receptors (Wulfetange et al., 2011) localised at the ER membrane.

Importantly, similar gradient pattern (higher IAA enrichment in ER compared to nuclei) of isotopically labelled IAA between ER and nuclei was observed as in case of endogenous IAA distribution within these two organelles (Figures 4a and 5a). Včelařová et al. (2021) previously showed the enrichment of IAA levels in isolated ER compared to crude extract due to the activity of auxin transporters PIN-FORMED 5 and PIN-LIKESs (Casanova-Sáez et al., 2021). However, it is not clear how ER-localised transporters are involved in the regulation of IAA flux into the nuclei, a fundamental step for auxin signalling (Middleton et al., 2018). The presence of IAA catabolites in the nucleus could imply inactivation of IAA in this organelle while transport of IAA catabolites in the nucleus cannot be excluded. Moreover, Hayashi et al. (2021) and Müller et al. (2021) recently provided data that modifies the IAA inactivation pathways suggesting IAA conjugation, followed by oxidation to (for example) oxIAA-Asp, followed by hydrolysis to give oxIAA or vice versa Figure 4b (Brunoni et al., 2023). In brief, these two pathways complement each other, and they are not separated as it was expected previously. However, this mingling suggests complex regulatory mechanisms of auxin homeostasis and fine-tuning of IAA levels. In general, it still remains unanswered whether the detected pool of phytohormone-related compounds is created by biosynthesis or by transport system. In case of CKs, their intracellular transport is still unknown despite of the recently discovered AZG2 ER transporter (Tessi et al., 2021).

In summary, it should be noted that the first intracellular hormone maps presented here (Figure 4) derive from individual and independent cells as plant cell cultures have been used. Future FAmOS work with samples from plant tissues and specific organs will shed light on the role of specific phytohormone transporters, receptors and metabolic enzymes in developmental processes. A significant advantage of the FAmOS method is that it can be directly applied in different mutant and overexpressing transgenic lines, as well as in different plant species. It can also be combined with various downstream applications, such as proteomics, metabolomics and transcriptomics. This ground-breaking method has strong potential to improve our understanding of the role of different organelles during plant development, and further method development, using cell- and organelle-type specific marker lines, will be very useful for studies of specific developmental processes in plants. In a future perspective, a more complete picture of phytohormone distribution at the (sub)cellular level should include other compartments together with cytosolic and apoplastic fluids.

EXPERIMENTAL PROCEDURES

Plant material and growth conditions

Arabidopsis (*Arabidopsis thaliana*) Col-0 cell suspension cultures originated from root tissue (Pesquet et al., 2010) were grown in liquid Murashige and Skoog media supplemented with 3% sucrose, pH adjusted to 5.7, in darkness at 22°C. Plant cells were weekly subcultured into fresh media in ratio of 1:10. Seven-day-old and 14-day-old cells cultivated under continuous light with fully-developed chloroplasts (Dubreuil et al., 2018) were used for confocal microscopy. Fourteen-day-old cells with chloroplasts were used for all control and sorting experiments. *A. thaliana* lines expressing organelle-specific markers: *β-ATPase:GFP* in mitochondria (Logan & Leaver, 2000), *HDEL:GFP* in ER (Matsushima et al., 2002) and *H2B:YFP* in nuclei (Boisnard-Lorig et al., 2001) were utilized for confocal microscopy and for organelle sorting (FAmOS gating strategy verification; see below). Seeds were sterilized in 70% ethanol with 0.01% Tween-20 for 10 min, then rinsed five times with sterile water and sown on square Petri dishes containing solid Murashige and Skoog medium with 1% sucrose, 2.5 mM 2-(*N*-morpholino)ethanesulfonic acid (MES) and 1% agar. After stratification in darkness at 4°C, seeds were placed vertically in a growth chamber for 5 days (for confocal microscopy) or 10 days (for sorting) in long-day conditions (16 h light and 8 h darkness) at 22°C.

Protoplast isolation and staining with fluorescent dyes

Roots of 5-day-old Arabidopsis transgenic lines *β-ATPase:GFP*, *HDEL:GFP* and *H2B:YFP* were separately harvested and

immediately submerged into protoplast isolation buffer. Their root protoplasts were extracted as described in ref. (Yoo et al., 2007) with slight modifications according to ref. (Antoniadi et al., 2015). The isolated protoplasts from each line were stained with the corresponding fluorescent dye that would label the same organelle endogenously expressing GFP or YFP according to the transgene. Therefore, root protoplasts originated from *β-ATPase:GFP* line were treated with 0.1 μM MitoTracker Orange CMTMRos (Thermo Fisher Scientific, Waltham, MA, USA; double labelling of mitochondria), the ones from *HDEL:GFP* line with 1 μM ER-Tracker Red (Thermo Fisher Scientific, Waltham, MA, USA; double labelling of ER) and from *H2B:YFP* line with 1 μg/ml Hoechst 33342 (Thermo Fisher Scientific, Waltham, MA, USA; double labelling of nuclei). After 10 min of staining, the microscopy slides were covered with a thin layer of poly-L-lysine, and the confocal imaging took place. Wild-type protoplasts from the cell culture cultivated under light conditions were also isolated and stained with all dyes simultaneously (0.1 μM MitoTracker Orange CMTMRos, 1 μM ER-Tracker Green and 1 μg/ml Hoechst 33342) to image the dyes' specificity and spectra overlap, including the autofluorescence in chloroplasts.

Confocal microscopy

For confocal experiments imaging protoplasts co-stained with a mixture of fluorescent dyes, fluorescence was recorded using a Zeiss LSM 880 inverted fast Airyscan microscope (Carl Zeiss AG, Oberkochen, Germany) with the objective C-Apochromat 40x NA 1.20 W Korr FCS M27. The pinhole was set to 183.2 μm, and the images were taken in two fluorescence tracks. Track 1 included ER-Tracker Green or GFP or YFP and chlorophyll excitations with 488 nm blue laser and respective emissions detection between 499–535 nm and 638–721 nm, respectively. Track 2 accommodated excitations of Hoechst 33342 (405 nm violet laser) which is more permeable through plasma membrane in comparison to Hoechst 33258 used in FAmOS and MitoTracker Orange CMTMRos (561 nm yellow-green laser) with respective emissions detected between 410–483 nm and 570–633 nm.

For confocal experiments imaging co-localization of the fluorescent dye and endogenous fluorescent of transgenic GFP lines, fluorescence was recorded using a Zeiss LSM 780 CLSM with an inverted microscope. The objective used was C-Apochromat 40×/1.20 W Korr M27, and the parameters are shown in Figure S1b.

Sample preparation for FAmOS

An aliquot of light-grown cell culture (2 ml) was pelleted by gravity at room temperature. Due to the large clusters (up to 100 cells), the concentration of cells in the suspension culture was not determined. During the following steps, all components were kept on ice, and all manipulations were performed with precooled equipment. Cells were washed twice with 0.7% NaCl and then ground in 0.7% NaCl supplemented with 1 mM phenylmethanesulfonyl fluoride (PMSF) and phosphatase inhibitor cocktail (final concentrations: 1 mM Na_3VO_4, 4 mM sodium tartrate dibasic dihydrate, 10 mM NaF, 1 mM Na_2MoO_4, 5 mM glycerol 2-phosphate disodium salt hydrate, 1 mM sodium pyrophosphate decahydrate) in a glass tube with Potter-Elvehjem PTFE pestle by 15 strokes. Released organelles were filtered through two layers of prewetted Miracloth to remove unbroken cells, big aggregates and cell debris. Finally, 1 ml of the resulting organelle suspension was stained with the mix of fluorescent dyes (final concentrations: 1 μM ER-Tracker Green, 0.1 μM Mitotracker Orange CMTMRos and 0.2 μg/ml Hoechst 33258) for 10 min in the dark. The sample was filtered again through one layer of prewetted Miracloth prior to injection into the flow cytometer.

Organelle analysis, gating and sorting

Fluorescently-stained organelles were analysed and sorted using a BD FACS Aria III flow cytometer equipped with four lasers: violet (405 nm), blue (488 nm), yellow-green (561 nm) and red (633 nm) lasers (BD Biosciences, San Jose, CA, USA). BD FACSDiva software version 7.0 was used for cytometer handling and data analysis. Organelle suspension was loaded in the cell sorter (4°C, mild agitation of 100 rpm) and forced through the cuvette in a single-file stream, where laser lights intercepted the stream at the sample interrogation point. After passing through the cuvette, the stream entered the integrated 85 μm nozzle tip, where the drop drive broke the stream into the droplets for sorting. Detection and recording of the interrogated particles deriving from the organelle suspension took place as described in Figure S1c. The forward scatter (FSC) of light was initially filtered through a 1.5 neutral density filter and then perceived by a photodiode detector with a 488/10 bandpass filter.

The sorted samples were collected in polypropylene tubes kept at 4°C during the sorting process. Simultaneous sorting of four organelle populations required additional optimization. The sheath fluid 0.7% NaCl that has been so far used for its compatibility with downstream LC-MS/MS applications (Antoniadi et al., 2015) lacked the appropriate viscosity for the required four-way sorting process. Therefore, we have changed the sheath fluid composition to 70% FACS Flow (BD Bioscience, San Jose, CA, USA) to ensure balance between viscosity and LC-MS/MS affinity.

Additional confidence for the selected fluorochrome separation was also derived by the cell sorter instrument armed with four lasers strategically built in a spatial sequence. The fluorescence emission caused by the excitation of the four spatially separated lasers is perceived by a distinct detector equipped with several bandpass filters. This means that each of the lasers has a specific detector with its own set of band pass filters. Combining the above criteria and sorting possibilities drove our selection into the following fluorescent dyes: Hoechst, ER-tracker Green and MitoTracker Orange CMTMRos excited by UV, Blue and Yellow-Green lasers, respectively (Figure S1a,c). Chlorophyll is excited mainly with the blue laser, the same as ER-tracker Green. However, the two fluorophores emit fluorescence in different wavelengths that are further narrowed down by bandpass filters and can thus be separated during flow cytometry (Figure S1a,c).

The relevant size estimation of the particles analysed was facilitated by calibration beads with known diameters (2, 3 and 6 μm). For ER, mitochondria and nuclei, unstained samples were used as negative controls, while for chloroplasts, we prepared a negative control organelle suspension from cells cultivated in the dark, thus lacking chlorophyll (Figure S2).

The selection of mitochondria as the last population for identification during our gating strategy (after exclusion of debris, aggregates, chloroplasts, nuclei and ER, Figure S2) was not random. Mitochondria proved challenging to clearly distinguish from background noise over sorting time due to the fluorescent signal intensity of MitoTracker dye's rapid deterioration. As a result, the number of identified mitochondria decreased significantly after 10 min of sorting. Our strategies to resolve this issue included both the above-mentioned fine design of their gate, where mitochondria were the last and most filtered designed gate, and also the time reduction between sample preparation and sorting to the minimum possible (Figure S4).

Finally, during FAmOS, organelle sorting can be live monitored, documented and in parallel analysed by several parameters. For example, data generated during FAmOS include the number of

particles that passed before the laser, their relative size and granularity/complexity, and their (auto)fluorescent signal intensities. These values can be used for further calculations (organelle yield) or normalized data projection (number of organelles sorted). Crucially, in this method, one can always return to inspect the data derived from a specific sorted and analysed sample.

FAmOS gating strategy verification

The gating strategy was verified by preparing organelle suspensions from the plant lines expressing GFP or YFP in selected organelles, as shown in Figure 1a. Before the flow cytometry analysis, the endogenously fluorescent organelle suspensions were additionally stained with the individual respective fluorescent dye. This resulted in double staining of a specific organelle by both GFP/YFP and fluorescent dye of different emission and/or excitation. Since both signals corresponded to the already created gates, the identity of the appropriate populations was verified. Ultimately, this also provided a proof of concept for our gating strategy as simultaneous isolation of chloroplasts, nuclei, ER and mitochondria was achieved (Figure 1c).

Protoplast and vacuole isolation

Protoplasts and vacuoles were isolated from 14-day-old suspension cells in accordance with the modified protocol from Robert et al. (2007). Ten millitres of suspension cells were sedimented by gravity, and the medium was removed. Cells were resuspended in a 30 ml enzyme solution containing 0.3 units/ml pectolyase and 45 units/ml cellulysin, 27 mM $CaCl_2$, 10 mM MES pH 5.6, 0.4 M mannitol without β-mercaptoethanol for 4 h in the dark. At the beginning of the incubation, a vacuum was applied to the cell suspension for 1 min. For the feeding experiment, the cell suspension was treated with 10 μM [$^{13}C_6$]IAA, 10 μM [$^{15}N_4$]iP, or 96% ethanol as mock and incubated for 2 h. Protoplasts were then passed through a 100 μm collector tissue sieve, washed twice and collected by gentle centrifugation (at 200 × ***g*** at 20 °C for 20 min). Protoplasts were lysed by adding the lysis buffer (0.2 M Mannitol, 10% Ficoll, 5 mM sodium phosphate pH 8, 10 mM EDTA pH 8, 0.0005% Neutral Red) and pipetting 5 times up and down. Released vacuoles were purified through a three-step Ficoll gradient by ultracentrifugation at 71 000 × ***g*** at 10°C for 55 min. Numbers of protoplasts or vacuoles were calculated using the Bürker counting chamber. All collected samples were immediately frozen in liquid nitrogen and stored at −80°C until further analysis.

The SDS-PAGE Immunoblot assay

Immunoblot analysis was performed as described in ref. (Včelařová et al., 2021). Briefly, sorted samples were concentrated on 3 kDa Amicon filters. Protein samples were mixed with Laemmli Sample Buffer supplemented with 10% β-mercaptoethanol. Protein mixtures were separated on 12% polyacrylamide gel and transferred onto 0.45 μm nitrocellulose membrane. The membrane was blocked with 5% low-fat milk in TBS-T for 1 h, cut into segments, which were incubated for 1 h with respective primary antibody (Agrisera, Vännäs, Sweden) against the organelle markers listed below: anti-H3 (1:5000; AS10 710), anti-PsbA (1:10000; AS05 084), anti-CNX1/2 (1:2500; AS12 2365), anti-GDC-H (1:5000; AS05 074) and anti-Sec21p (1:1000; AS08 327). Pieces of membranes were then incubated with goat anti-rabbit IgG (H&L) HRP-conjugated secondary antibody (1:10 000; AS09 602). Marker proteins were visualized using a chemiluminescence kit (SuperSignal™ West Pico Chemiluminescent Substrate, Thermo Fisher Scientific, Waltham, MA, USA) using a ChemiDoc MP Imaging System (Bio-Rad, Hercules, CA, USA). A total protein extract from *A. thaliana* using SDS buffer was prepared as a positive control.

Control experiments

Organelle suspension was prepared as described above and treated with either 3 mM NaN_3, 10 μM adenine, 40 μM 1-*N*-naphtylphthalamic acid, 10 μM adenosine 5′-monophosphate, a phosphatase inhibitor cocktail (as described in sample preparation), a mixture of fluorescent dyes (as described in sample preparation) or DMSO as control. The samples were incubated on ice in the dark to imitate the sorting process for 0, 30 min, 1 and 2 h and were frozen in liquid nitrogen.

Formaldehyde mild fixation was done as published in ref. (Petrovská et al., 2014). Briefly, cells were fixed with 2% formaldehyde for 10 min on ice. Cells were washed with deionised water and frozen in liquid nitrogen.

For the final overview of phytohormone profile stability during (I) sample preparation and (II) sorting, *in vivo* labelling experiments were performed. Organelle suspension was prepared as described above. However, 2 h before grinding, cells were spiked with 10 μM [$^{15}N_4$]iP and [$^{13}C_6$]IAA. Organelle suspension was aliquoted and frozen in liquid nitrogen after 15 min of incubation, imitating sample preparation.

The prepared sample for FAmOS (as described above) was directly spiked with 10 μM [$^{15}N_4$]iP and [$^{13}C_6$]IAA before sample injection into the flow cytometer. Each organelle population (200 000 organelles) was sorted from the treated organelle suspension. The sorted samples were pooled together, and then divided into aliquots comprising 200 000 organelles to achieve even distribution of organelle types and frozen in liquid nitrogen. The above-mentioned control experiments are schematically represented in Figure S4b. All samples were stored at −80°C until auxin and CK analysis.

Auxin and cytokinin analysis

Auxins and CKs were purified according to the in-tip solid-phase microextraction protocol described by ref. (Svačinová et al., 2012) with modification according to Antoniadi et al. (2015). Firstly, samples were thawed on ice, aliquoted into 200 000 sorted organelles or vacuoles, and frozen in liquid nitrogen to rupture membranes. Samples were diluted with deionised water at a ratio of 3:1 (v/v) and acidified with 1 M HCl to pH≤2.7. Prior to extraction isotope-labelled internal standards (Olchemim, Olomouc, Czech Republic) were added to each sample as follows: 0.5 pmol of [$^{13}C_6$]IAA, [$^{13}C_6$]oxIAA, [$^{13}C_6$]IAA-Asp, [$^{13}C_6$]IAA-Glu, [$^{13}C_6$]IAA-glc, [$^{13}C_6$]oxIAA-glc; 0.2 pmol of [$^{13}C_5$]cZ, [$^{13}C_5$]tZ, [$^{2}H_3$]DHZ, [$^{2}H_6$]iP, [$^{2}H_5$]tZR, [$^{2}H_3$]DHZR, [$^{2}H_6$]iPR, [$^{2}H_5$]tZ7G, [$^{15}N_4$]cZ7G, [$^{2}H_6$]iP7G, [$^{2}H_5$]tZ9G, [$^{2}H_3$]DHZ9G and [$^{2}H_6$]iP9G; 0.5 pmol of [$^{2}H_5$]tZOG, [$^{2}H_7$]DHZOG, [$^{2}H_5$]tZROG, [$^{2}H_5$]tZRMP, [$^{2}H_3$]DHZRMP and [$^{2}H_6$]iPRMP. After loading the sample onto the microcolumn, sorbent with analytes was washed with deionised water, and auxins were eluted with methanol and CKs with 0.5 mM NH_4OH in 60% (v/v) methanol. Eluates were evaporated to dryness and then dissolved in 10% methanol. Auxin and CKs contents were determined by ultra-performance liquid chromatography coupled with electro-spray-tandem mass spectrometry using a 1290 Infinity LC - 6495Triple Quadrupole LC/MS systems (Agilent Technologies, Santa Clara, CA, USA) and an Acquity UPLC I-Class - Xevo TQ-S MS systems (Waters, Milford, MA, USA), respectively, as described in ref. (Pěnčík et al., 2018; Svačinová et al., 2012), respectively. Data were normalized according to the protein content of organelle fraction (Table S1), and the phytohormone maps were expressed as the

ratio of compound(s) level in particular organelle to compound(s) level in chloroplasts. To specifically estimate the ratio of CK *O*-glucosides and IAA amino acid-conjugates in vacuoles compared to chloroplasts, the missing values of the targeted compounds in chloroplasts were replaced with two-thirds of their respective detection limit (Martín-Fernández et al., 2003) normalized per protein amount (listed in Table S4). Labelled and endogenous phytohormone metabolites after organelle-suspension treatment with [$^{15}N_4$]iP and [$^{13}C_6$]IAA were also isolated by in-tip solid-phase microextraction and measured using LC-MS/MS, with the multiple reaction monitoring transitions as described above. Importantly, [$^{13}C_6$]IAA and its metabolites were quantified using deuterium-labelled internal standards (2.5 pmol per sample) added prior to the extraction step.

Proteomic analysis

The sorted samples (organelle suspensions) were first concentrated employing a centrifugal filter unit with a 3 K cut-off. Then, proteins were precipitated by four volumes of ice-cold acetone. Protein pellets were collected by centrifugation and digested in-solution with commercially available trypsin as previously described (Leon et al., 2013). The resultant digests were purified using a homemade reversed-phase (C18) microcolumn as published in ref. (Franc et al., 2012) and subjected to LC-MS/MS analysis using a nanocapillary liquid chromatography system coupled to a tandem mass spectrometer UHR-QTOF maXis (Bruker Daltonics, Bremen, Germany) with settings adapted from ref. (Chamrád et al., 2014). The acquired MS data were processed for protein identification using MaxQuant software version 1.6.10.43 (Tyanova et al., 2016) with an instrument parameter setting "Bruker QTOF" (Beck et al., 2015) and Andromeda search engine (Cox et al., 2011). The data were searched against the *Arabidopsis thaliana* (cv. Columbia) protein database (UniProt, reference proteome UP000006548, 39 346 protein sequences, downloaded 2019/07/25) supplemented with 247 common laboratory contaminant proteins. To evaluate the relative abundances of the identified proteins, the intensity-based absolute quantification (iBAQ) method (Schwanhäusser et al., 2011) was utilized. To determine the enriched functional annotation themes (particularly GO terms) connected with the identified proteins, DAVID Bioinformatics Resources 6.8 (Huang et al., 2009) was used. The total protein content of the analysed samples was calculated from the MS data by integrating the area under the curve of the corresponding chromatogram. To this end, a series of protein digests with pre-set protein content prepared from *A. thaliana* cell culture was employed as a calibration (Včelařová et al., 2021) (Figure S3b). The MS/MS proteomics data have been deposited to the ProteomeXchange Consortium (http://proteomecentral.proteomexchange.org) via the PRIDE partner repository (Perez-Riverol et al., 2019) with the dataset identifier PXD033255. "*For the peer review process, please use following PRIDE account details - username*: reviewer_pxd033255@ebi.ac.uk; *password: yLoNvXGb.*" The original protein identification results with all relevant characteristics as provided by the MaxQuant software are attached in the Supporting Data S1-S6.

ACKNOWLEDGEMENTS

This work was supported by the Czech Science Foundation (20-22875S) and by the Internal Grant Agency of Palacký University in Olomouc (IGA_PrF_2023_031). V.S. was partially supported by the Endowment fund of Palacký University in Olomouc. The authors also acknowledge the European Molecular Biology Organization (EMBO ASTF 297-2013) (I.A.) and Plant Fellows (the International Post doc Fellowship Program in Plant Sciences, GA-2010-267423) (I.A.; K.L.). K.L. acknowledge the the Swedish Research Council (VR 2018-04235), Vinnova (2016-00504), Knut and Alice Wallenberg Foundation (KAW 2016.0341 and KAW 2016.0352) and Kempestiftelserna (SMK-1745). The authors would like to thank Tamara Hernández-Verdeja, and Åsa Strand for providing of Arabidopsis cell culture, Hélène S. Robert, Stéphanie Robert, Colin Turnbull for careful language revision, critical proof-reading and helpful comments, and to Ota Blahoušek for graphic editing of figures. We also thank the Swedish Metabolomics Centre for the use of instrumentation.

AUTHOR CONTRIBUTIONS

VS, IA, MFK, MS, KJ and ON developed the idea and outline of the paper; VS, IA, AP, IC, RL, MFK, MZ, AŽ and ON performed experiments and data analysis; VS, IA, AP, IC, MS, KL and ON discussed results and create outline of the paper; MS, KL and ON supervised the project; VS, IA, IC and ON wrote the manuscript with input from all authors. All authors have read and agreed to the published version of the manuscript.

CONFLICT OF INTEREST

The authors declare no conflict of interests.

DATA AVAILABILITY STATEMENT

The data that support the findings of this study are available from the corresponding authors upon reasonable request. The proteomics data were deposited to the ProteomeXchange Consortium via the PRIDE partner repository with the dataset identifier PXD033255.

SUPPORTING INFORMATION

Additional Supporting Information may be found in the online version of this article.

Data S1. The Protein Groups table contains information on the identified proteins in the processed raw files. Each single row contains a group of proteins that could be reconstructed from a set of peptides. The file contains all the requested information about peptide and protein identification like the number of peptides used for protein identification, their sequences, protein sequence coverage and other important identification results. All detailed information about the identification of peptides is summarized in the Data S2 file.

Data S2. The peptides table contains information on the identified peptides in the processed raw files.

Data S3. The evidence file combines all the information about the identified peptides and normally is the only file required for processing the results.

Data S4. The summary file contains summary information for all the raw files processed with a single MaxQuant run.

Data S5. The TXT file describes the complete list of all parameters that were applied for processing all raw files by a MaxQuant run.

Data S6. The pdf file contains tables WITH the complete description of all information in the attached Data S1-S5 files and also includes the description of all column names.

Data S7. All quantification data of phytohormone levels in evaluation experiments and in organelle-enriched fractions.

Figure S1. Characteristics of selected fluorescent dyes.

Figure S2. Scheme of the gating strategy and isolation of the organelle populations.

Figure S3. Identity confirmation of the sorted organelle populations.

Figure S4. Scheme of FAmOS workflow and control experiments.

Figure S5. Evaluation of phytohormone profile stability.

Figure S6. Subcellular distribution of three isoprenoid CK groups within the Arabidopsis suspension cell.

Table S1. Protein content for sorted plant organelle fractions.

Table S2. Phytohormone levels in 1 000 000 sorted organelles (fmol/1000000 organelles).

Table S3. Phytohormone levels in aliquot of A. thaliana Col-0 cell culture (fmol or pmol/1 ml of cell culture).

Table S4. Phytohormone levels in organelle-enriched fractions (pmol/μg of proteins).

Table S5. Phytohormone levels (pmol/μg of proteins) in the organelle-enriched fractions isolated from Arabidopsis cell culture suspension and treated with 10 μM [$^{13}C_6$]IAA or 10 μM [$^{15}N_4$]iP.

REFERENCES

Adan, A., **Alizada, G.**, **Kiraz, Y.**, **Baran, Y.** & **Nalbant, A.** (2017) Flow cytometry: basic principles and applications. *Critical Reviews in Biotechnology*, **37**, 163–176. Available from: https://pubmed.ncbi.nlm.nih.gov/26767547/

Antoniadi, I., **Plačková, L.**, **Simonovik, B.**, **Doležal, K.**, **Turnbull, C.**, **Ljung, K.** ***et al.*** (2015) Cell-type-specific cytokinin distribution within the Arabidopsis primary root apex. *Plant Cell*, **27**, 1955–1967. Available from: http://www.pubmedcentral.nih.gov/articlerender.fcgi?artid=4531351&tool=pmcentrez&rendertype=abstract

Band, L.R., **Wells, D.M.**, **Fozard, J.A.**, **Ghetiu, T.**, **French, A.P.**, **Pound, M.P.** ***et al.*** (2014) Systems analysis of auxin transport in the Arabidopsis root apex. *Plant Cell*, **26**, 862–875. Available from: https://pubmed.ncbi.nlm.nih.gov/24632533/

Beck, S., **Michalski, A.**, **Raether, O.**, **Lubeck, M.**, **Kaspar, S.**, **Goedecke, N.** ***et al.*** (2015) The impact II, a very high-resolution quadrupole time-of-flight instrument (QTOF) for deep shotgun proteomics. *Molecular & Cellular Proteomics*, **14**, 2014–2029. Available from: https://pubmed.ncbi.nlm.nih.gov/25991688/

Boisnard-Lorig, C., **Colon-Carmona, A.**, **Bauch, M.**, **Hodge, S.**, **Doerner, P.**, **Bancharel, E.** ***et al.*** (2001) Dynamic analyses of the expression of the HISTONE::YFP fusion protein in arabidopsis show that syncytial endosperm is divided in mitotic domains. *Plant Cell*, **13**, 495–509. Available from: http://www.ncbi.nlm.nih.gov/pubmed/11251092

Boussardon, C., **Przybyla-Toscano, J.**, **Carrie, C.** & **Keech, O.** (2020) Tissue-specific isolation of Arabidopsis/plant mitochondria- IMTACT (isolation of mitochondria tagged in specific cell types). *The Plant Journal*, **103**, 459–473. Available from: http://www.ncbi.nlm.nih.gov/pubmed/32057155

Breitkopf, S.B., **Oppermann, F.S.**, **Kéri, G.**, **Grammel, M.** & **Daub, H.** (2010) proteomics analysis of cellular imatinib targets and their candidate downstream effectors. *Journal of Proteome Research*, **9**, 6033–6043. Available from: https://doi.org/10.1021/pr1008527

Brenner, W.G., **Ramireddy, E.**, **Heyl, A.** & **Schmülling, T.** (2012) Gene regulation by cytokinin in Arabidopsis. *Frontiers in Plant Science*, **3**, 8. Available from: https://pubmed.ncbi.nlm.nih.gov/22639635/

Brunoni, F., **Pěnčík, A.**, **Žukauskaitė, A.**, **Ament, A.**, **Kopečná, M.**, **Collani, S.** ***et al.*** (2023) Amino acid conjugation of oxIAA is a secondary metabolic regulation involved in auxin homeostasis. *New Phytologist*, **238**, 2264–2270. Available from: https://pubmed.ncbi.nlm.nih.gov/36941219/

Cancé, C., **Martin-Arevalillo, R.**, **Boubekeur, K.** & **Dumas, R.** (2022) Auxin response factors are keys to the many auxin doors. *The New Phytologist*, **235**, 402–419. Available from: https://pubmed.ncbi.nlm.nih.gov/35434800/

Carter, A.D., **Bonyadi, R.** & **Gifford, M.L.** (2013) The use of fluorescence-activated cell sorting in studying plant development and environmental responses. *The International Journal of Developmental Biology*, **57**, 545–552. Available from: https://pubmed.ncbi.nlm.nih.gov/24166437/

Casanova-Sáez, R., **Mateo-Bonmatí, E.** & **Ljung, K.** (2021) Auxin metabolism in plants. *Cold Spring Harbor Perspectives in Biology*, **13**, a039867. Available from: https://pubmed.ncbi.nlm.nih.gov/33431579/

Cedzich, A., **Stransky, H.**, **Schulz, B.** & **Frommer, W.B.** (2008) Characterization of cytokinin and adenine transport in Arabidopsis cell cultures. *Plant Physiology*, **148**, 1857–1867. Available from: https://pubmed.ncbi.nlm.nih.gov/18835995/

Chamrád, I., **Simerský, R.**, **Bérešová, L.**, **Strnad, M.**, **Šebela, M.** & **Lenobel, R.** (2014) Proteomic identification of a candidate sequence of wheat cytokinin-binding protein 1. *Journal of Plant Growth Regulation*, **33**, 896–902.

Cox, J., **Neuhauser, N.**, **Michalski, A.**, **Scheltema, R.A.**, **Olsen, J.V.** & **Mann, M.** (2011) Andromeda: A peptide search engine integrated into the MaxQuant environment. *Journal of Proteome Research*, **10**, 1794–1805. Available from: https://pubmed.ncbi.nlm.nih.gov/21254760/

Deal, R.B. & **Henikoff, S.** (2011) The INTACT method for cell type–specific gene expression and chromatin profiling in Arabidopsis thaliana. *Nature Protocols*, **6**, 56–68. Available from: http://www.ncbi.nlm.nih.gov/pubmed/21212783

Di Mambro, R., **De Ruvo, M.**, **Pacifici, E.**, **Salvi, E.**, **Sozzani, R.**, **Benfey, P.N.** ***et al.*** (2017) Auxin minimum triggers the developmental switch from cell division to cell differentiation in the Arabidopsis root. *Proceedings of the National Academy of Sciences of the United States of America*, **114**, E7641–E7649. Available from: http://www.ncbi.nlm.nih.gov/pubmed/28831001

Di Mambro, R., **Svolacchia, N.**, **Ioio, R.D.**, **Pierdonati, E.**, **Salvi, E.**, **Pedrazzini, E.** ***et al.*** (2019) The lateral root cap acts as an auxin sink that controls meristem size. *Current Biology*, **29**, 1199–1205.e4. Available from: http://www.ncbi.nlm.nih.gov/pubmed/30880016

Dubreuil, C., **Jin, X.**, **Barajas-López, J.D.D.** ***et al.*** (2018) Establishment of photosynthesis through chloroplast development is controlled by two distinct regulatory phases. *Plant Physiology*, **176**, 1199–1214. Available from: https://doi.org/10.1104/pp.17.00435

Franc, V., **Šebela, M.**, **Řehulka, P.**, **Končitíková, R.**, **Lenobel, R.**, **Madzak, C.** ***et al.*** (2012) Analysis of N-glycosylation in maize cytokinin oxidase/dehydrogenase 1 using a manual microgradient chromatographic separation coupled offline to MALDI-TOF/TOF mass spectrometry. *Journal of Proteomics*, **75**, 4027–4037. Available from: https://pubmed.ncbi.nlm.nih.gov/22634084/

Friml, J., **Vieten, A.**, **Sauer, M.**, **Weijers, D.**, **Schwarz, H.**, **Hamann, T.** ***et al.*** (2003) Efflux-dependent auxin gradients establish the apical-basal axis of Arabidopsis. *Nature*, **426**, 147–153. Available from: http://www.nature.com/articles/nature02085

Galbraith, D., **Loureiro, J.**, **Antoniadi, I.**, **Bainard, J.**, **Bureš, P.**, **Cápal, P.** ***et al.*** (2021) Best practices in plant cytometry. *Cytometry Part A*, **99**, 311–317. https://doi.org/10.1002/cyto.a.24295

Haas, C., **Hegner, R.**, **Helbig, K.**, **Bartels, K.**, **Bley, T.** & **Weber, J.** (2016) Two parametric cell cycle analyses of plant cell suspension cultures with fragile, isolated nuclei to investigate heterogeneity in growth of batch cultivations. *Biotechnology and Bioengineering*, **113**, 1244–1250. Available from: https://pubmed.ncbi.nlm.nih.gov/26614913/

Hayashi, K., **Arai, K.**, **Aoi, Y.** ***et al.*** (2021) The main oxidative inactivation pathway of the plant hormone auxin. *Nature Communications*, **12**, 1–11. Available from: https://www.nature.com/articles/s41467-021-27020-1

Hayashi, K., **Nakamura, S.**, **Fukunaga, S.**, **Nishimura, T.**, **Jenness, M.K.**, **Murphy, A.S.** ***et al.*** (2014) Auxin transport sites are visualized in planta using fluorescent auxin analogs. *Proceedings of the National Academy of Sciences of the United States of America*, **111**, 11557–11562. Available from: https://doi.org/10.1073/pnas.1408960111

Hošek, P., **Hoyerová, K.**, **Kiran, N.S.**, **Dobrev, P.I.**, **Zahajská, L.**, **Filepová, R.** ***et al.*** (2020) Distinct metabolism of N-glucosides of isopentenyladenine and trans-zeatin determines cytokinin metabolic spectrum in Arabidopsis. *The New Phytologist*, **225**, 2423–2438. Available from: https://pubmed.ncbi.nlm.nih.gov/31682013/

Hoyerová, K., **Gaudinová, A.**, **Malbeck, J.**, **Dobrev, P.I.**, **Kocábek, T.**, **Šolcová, B.** ***et al.*** (2006) Efficiency of different methods of extraction and purification of cytokinins. *Phytochemistry*, **67**, 1151–1159. Available from: https://pubmed.ncbi.nlm.nih.gov/16678229/

Huang, D.W., **Sherman, B.T.** & **Lempicki, R.A.** (2009) Systematic and integrative analysis of large gene lists using DAVID bioinformatics resources. *Nature Protocols*, **4**, 44–57. Available from: https://pubmed.ncbi.nlm.nih.gov/19131956/

Huber, L.A., **Pfaller, K.** & **Vietor, I.** (2003) Organelle proteomics: implications for subcellular fractionation in proteomics. *Circulation Research*, **92**, 962–968. Available from: http://www.ncbi.nlm.nih.gov/pubmed/12750306

Hurný, A., **Cuesta, C.**, **Cavallari, N.**, **Ötvös, K.**, **Duclercq, J.**, **Dokládal, L.** ***et al.*** (2020) SYNERGISTIC ON AUXIN AND CYTOKININ 1 positively regulates growth and attenuates soil pathogen resistance. *Nature Communications*, **11**, 2170. Available from: https://pubmed.ncbi.nlm.nih.gov/32358503/

Jiskrová, E., **Novák, O.**, **Pospíšilová, H.**, **Holubová, K.**, **Karády, M.**, **Galuszka, P.** ***et al.*** (2016) Extra- and intracellular distribution of cytokinins in the leaves of monocots and dicots. *New Biotechnology*, **33**, 735–742. Available from: https://pubmed.ncbi.nlm.nih.gov/26777983/

Kakimoto, T. (2001) Identification of plant cytokinin biosynthetic enzymes as dimethylallyl diphosphate:ATP/ADP isopentenyltransferases. *Plant and Cell Physiology*, **42**, 677–685. Available from: http://www.ncbi.nlm.nih.gov/pubmed/11479373

Kasahara, H., **Takei, K.**, **Ueda, N.**, **Hishiyama, S.**, **Yamaya, T.**, **Kamiya, Y.** ***et al.*** (2004) Distinct isoprenoid origins of cis- and trans-zeatin biosyntheses in Arabidopsis. *The Journal of Biological Chemistry*, **279**, 14049–14054.

Kiran, N.S., **Benková, E.**, **Reková, A.**, **Dubová, J.**, **Malbeck, J.**, **Palme, K.** ***et al.*** (2012) Retargeting a maize β-glucosidase to the vacuole - Evidence from intact plants that zeatin-O-glucoside is stored in the vacuole. *Phytochemistry*, **79**, 67–77. Available from: https://pubmed.ncbi.nlm.nih.gov/22552277/

Kubiasová, K., **Montesinos, J.C.**, **Šamajová, O.**, **Nisler, J.**, **Mik, V.**, **Semerádová, H.** ***et al.*** (2020) Cytokinin fluoroprobe reveals multiple sites of cytokinin perception at plasma membrane and endoplasmic reticulum. *Nature Communications*, **11**, 4285. Available from: https://www.nature.com/articles/s41467-020-17949-0

Kurakawa, T., **Ueda, N.**, **Maekawa, M.**, **Kobayashi, K.**, **Kojima, M.**, **Nagato, Y.** ***et al.*** (2007) Direct control of shoot meristem activity by a cytokinin-activating enzyme. *Nature*, **445**, 652–655. Available from: http://www.ncbi.nlm.nih.gov/pubmed/17287810

Lee, Y.H., **Tan, H.T.** & **Chung, M.C.M.** (2010) Subcellular fractionation methods and strategies for proteomics. *Proteomics*, **10**, 3935–3956. Available from: http://www.ncbi.nlm.nih.gov/pubmed/21080488

Leon, I.R., **Schwammle, V.**, **Jensen, O.N.** & **Sprenger, R.R.** (2013) Quantitative assessment of in-solution digestion efficiency identifies optimal protocols for unbiased protein analysis. *Molecular & Cellular Proteomics*, **12**, 2992–3005. Available from: https://pubmed.ncbi.nlm.nih.gov/23792921/

Levi, M., **Tarquini, F.**, **Sgorbati, S.** & **Sparvoli, E.** (1986) Determination of DNA content by static cytofluorimetry in nuclei released from fixed plant tissue. *Protoplasma*, **132**, 64–68. Available from: https://doi.org/10.1007/BF01275791

Liao, C.Y., **Smet, W.**, **Brunoud, G.**, **Yoshida, S.**, **Vernoux, T.** & **Weijers, D.** (2015) Reporters for sensitive and quantitative measurement of auxin response. *Nature Methods*, **12**, 207–210. Available from: https://pubmed.ncbi.nlm.nih.gov/25643149/

Logan, D.C. & **Leaver, C.J.** (2000) Mitochondria-targeted GFP highlights the heterogeneity of mitochondrial shape, size and movement within living plant cells. *Journal of Experimental Botany*, **51**, 865–871. Available from: http://www.ncbi.nlm.nih.gov/pubmed/10948212

Martín-Fernández, J.A., **Barceló-Vidal, C.** & **Pawlowsky-Glahn, V.** (2003) Dealing with zeros and missing values in compositional data sets using nonparametric imputation. *Mathematical Geology*, **35**, 253–278.

Matsushima, R., **Hayashi, Y.**, **Kondo, M.**, **Shimada, T.**, **Nishimura, M.** & **Hara-Nishimura, I.** (2002) An endoplasmic reticulum-derived structure that is induced under stress conditions in Arabidopsis. *Plant Physiology*, **130**, 1807–1814. Available from: http://www.ncbi.nlm.nih.gov/pubmed/12481064

Mellor, N., **Band, L.R.**, **Pěnčík, A.**, **Novák, O.**, **Rashed, A.**, **Holman, T.** ***et al.*** (2016) Dynamic regulation of auxin oxidase and conjugating enzymes AtDAO1 and GH3 modulates auxin homeostasis. *Proceedings of the National Academy of Sciences of the United States of America*, **113**, 11022–11027. Available from: https://doi.org/10.1073/pnas.1604458113

Middleton, A.M., **Dal Bosco, C.**, **Chlap, P.**, **Bensch, R.**, **Harz, H.**, **Ren, F.** ***et al.*** (2018) Data-driven modeling of intracellular auxin fluxes indicates a dominant role of the ER in controlling nuclear auxin uptake. *Cell Reports*, **22**, 3044–3057. Available from: http://linkinghub.elsevier.com/retrieve/pii/S2211124718302699

Millar, A.H. & **Taylor, N.L.** (2017) The isolation of plant organelles and structures in the post-genomic era. *Methods in Molecular Biology*, **1511**, 1–11. Available from: https://pubmed.ncbi.nlm.nih.gov/27730598/

Müller, B. & **Sheen, J.** (2008) Cytokinin and auxin interaction in root stem-cell specification during early embryogenesis. *Nature*, **453**, 1094–1097. Available from: http://www.nature.com/articles/nature06943

Müller, K., **Dobrev, P.I.**, **Pencík, A.** ***et al.*** (2021) DIOXYGENASE FOR AUXIN OXIDATION 1 catalyzes the oxidation of IAA amino acid conjugates. *Plant Physiology*, **187**, 103–115. Available from: https://pubmed.ncbi.nlm.nih.gov/34618129/

Niehaus, M., **Straube, H.**, **Künzler, P.**, **Rugen, N.**, **Hegermann, J.**, **Giavalisco, P.** ***et al.*** (2020) Rapid affinity purification of tagged plant mitochondria (Mito-AP) for metabolome and proteome analyses. *Plant Physiology*, **182**, 1194–1210. Available from: https://pubmed.ncbi.nlm.nih.gov/31911558/

Novák, O., **Hényková, E.**, **Sairanen, I.**, **Kowalczyk, M.**, **Pospíšil, T.** & **Ljung, K.** (2012) Tissue-specific profiling of the Arabidopsis thaliana auxin metabolome. *The Plant Journal*, **72**, 523–536. Available from: https://doi.org/10.1111/j.1365-313X.2012.05085.x

Novák, O., **Napier, R.** & **Ljung, K.** (2017) Zooming in on plant hormone analysis: tissue- and cell-specific Approaches. *Annual Review of Plant Biology*, **68**, 323–348. Available from: http://www.ncbi.nlm.nih.gov/pubmed/28226234

Pavlova, P., **van Zanten, M.**, **Snoek, B.L.**, **Jong, H.d.** & **Fransz, P.** (2021) 2D morphometric analysis of Arabidopsis thaliana nuclei reveals characteristic profiles of different cell types and accessions. *Chromosome Research*, **30**, 5–24. Available from: https://pubmed.ncbi.nlm.nih.gov/34665365/

Pěnčík, A., **Casanova-Sáez, R.**, **Pilařová, V.**, **Žukauskaitė, A.**, **Pinto, R.**, **Luis Micol, J.** ***et al.*** (2018) Ultra-rapid auxin metabolite profiling for high-throughput mutant screening in Arabidopsis. *Journal of Experimental Botany*, **69**, 2569–2579. Available from: http://www.duchefa.com

Pěnčík, A., **Simonovik, B.**, **Petersson, S.V.**, **Henyková, E.**, **Simon, S.**, **Greenham, K.** ***et al.*** (2013) Regulation of auxin homeostasis and gradients in Arabidopsis roots through the formation of the indole-3-acetic acid catabolite 2-oxindole-3-acetic acid. *Plant Cell*, **25**, 3858–3870. Available from: https://doi.org/10.1105/tpc.113.114421

Perez-Riverol, Y., **Csordas, A.**, **Bai, J.**, **Bernal-Llinares, M.**, **Hewapathirana, S.**, **Kundu, D.J.** ***et al.*** (2019) The PRIDE database and related tools and resources in 2019: Improving support for quantification data. *Nucleic Acids Research*, **47**, D442–D450. Available from: https://pubmed.ncbi.nlm.nih.gov/30395289/

Pesquet, E., **Korolev, A.V.**, **Calder, G.** & **Lloyd, C.W.** (2010) The microtubule-associated protein AtMAP70-5 regulates secondary wall patterning in Arabidopsis wood cells. *Current Biology*, **20**, 744–749.

Petersson, S.V., **Johansson, A.I.**, **Kowalczyk, M.** ***et al.*** (2009) An auxin gradient and maximum in the Arabidopsis root apex shown by high-resolution cell-specific analysis of IAA distribution and synthesis. *Plant Cell*, **21**, 1659–1668. Available from: http://www.ncbi.nlm.nih.gov/pubmed/19491238

Petrášek, J., **Mravec, J.**, **Bouchard, R.** ***et al.*** (2006) PIN proteins perform a rate-limiting function in cellular auxin efflux. *Science*, **312**, 914–918. Available from: https://doi.org/10.1126/science.1123542

Petrovská, B., **Jeřábková, H.**, **Chamrád, I.**, **Vrána, J.**, **Lenobel, R.**, **Uřinovská, J.** ***et al.*** (2014) Proteomic analysis of barley cell nuclei purified by flow sorting. *Cytogenetic and Genome Research*, **143**, 78–86. Available from: https://www.karger.com/Article/FullText/365311

Polanská, L., **Vičánková, A.**, **Nováková, M.**, **Malbeck, J.**, **Dobrev, P.I.**, **Brzobohatý, B.** ***et al.*** (2007) Altered cytokinin metabolism affects cytokinin, auxin, and abscisic acid contents in leaves and chloroplasts, and chloroplast ultrastructure in transgenic tobacco. *Journal of Experimental Botany*, **58**, 637–649. Available from: https://doi.org/10.1093/jxb/erl235

Porco, S., **Pěnčík, A.**, **Rashed, A.**, **Voß, U.**, **Casanova-Sáez, R.**, **Bishopp, A.** ***et al.*** (2016) Dioxygenase-encoding AtDAO1 gene controls IAA oxidation and homeostasis in Arabidopsis. *Proceedings of the National Academy of Sciences of the United States of America*, **113**, 11016–11021. Available from: https://doi.org/10.1073/pnas.1604375113

Ranocha, P., **Dima, O.**, **Nagy, R.**, **Felten, J.**, **Corratgé-Faillie, C.**, **Novák, O.** ***et al.*** (2013) Arabidopsis WAT1 is a vacuolar auxin transport facilitator required for auxin homoeostasis. *Nature Communications*, **4**, 2625. Available from: https://doi.org/10.1038/ncomms3625

Robert, S., **Zouhar, J.**, **Carter, C.J.** & **Raikhel, N.** (2007) Isolation of intact vacuoles from Arabidopsis rosette leaf–derived protoplasts. *Nature Protocols*, **2**, 259–262. Available from: http://www.ncbi.nlm.nih.gov/pubmed/17406583

Sakakibara, H. (2006) Cytokinins: activity, biosynthesis, and translocation. *Annual Review of Plant Biology*, **57**, 431–449. Available from: https://pubmed.ncbi.nlm.nih.gov/16669769/

Schaller, G.E., **Bishopp, A.** & **Kieber, J.J.** (2015) The yin-yang of hormones: cytokinin and auxin interactions in plant development. *Plant Cell*, **27**, 44–63. Available from: https://doi.org/10.1105/tpc.114.133595

Schwanhäusser, B., **Busse, D.**, **Li, N.**, **Dittmar, G.**, **Schuchhardt, J.**, **Wolf, J.** ***et al.*** (2011) Global quantification of mammalian gene expression control. *Nature*, **473**, 337–342. Available from: https://pubmed.ncbi.nlm.nih.gov/21593866/

Šimášková, M., **O'Brien, J.A.**, **Khan, M.** ***et al.*** (2015) Cytokinin response factors regulate PIN-FORMED auxin transporters. *Nature Communications*, **6**, 8717. Available from: http://www.ncbi.nlm.nih.gov/pubmed/26541513

Skalický, V., **Kubeš, M.**, **Napier, R.** & **Novák, O.** (2018) Auxins and cytokinins-the role of subcellular organization on homeostasis. *International Journal of Molecular Sciences*, **19**, 3115. Available from: http://www.mdpi.com/1422-0067/19/10/3115

Skalický, V., **Vojtková, T.**, **Pěnčík, A.**, **Vrána, J.**, **Juzoń, K.**, **Koláčková, V.** ***et al.*** (2021) Auxin metabolite profiling in isolated and intact plant nuclei. *International Journal of Molecular Sciences*, **22**, 12369. Available from: https://www.mdpi.com/1422-0067/22/22/12369/htm

Šmehilová, M., **Dobrůšková, J.**, **Novák, O.**, **Takáč, T.** & **Galuszka, P.** (2016) Cytokinin-specific glycosyltransferases possess different roles in cytokinin homeostasis maintenance. *Frontiers in Plant Science*, **7**, 1264.

Suda, J., **Kron, P.**, **Husband, B.C.** & **Trávníček, P.** (2007) Flow cytometry and ploidy: applications in plant systematics, ecology and evolutionary biology. In: *Flow cytometry with plant cells*. Weinheim, Germany: Wiley, pp. 103–130. Available from: https://doi.org/10.1002/9783527610921.ch5

Svačinová, J., **Novák, O.**, **Plačková, L.**, **Lenobel, R.**, **Holík, J.**, **Strnad, M.** ***et al.*** (2012) A new approach for cytokinin isolation from Arabidopsis tissues using miniaturized purification: pipette tip solid-phase extraction. *Plant Methods*, **8**, 17.

Tessi, T.M., **Brumm, S.**, **Winklbauer, E.**, **Schumacher, B.**, **Pettinari, G.**, **Lescano, I.** ***et al.*** (2021) Arabidopsis AZG2 transports cytokinins in vivo and regulates lateral root emergence. *The New Phytologist*, **229**, 979–993. Available from: https://doi.org/10.1111/nph.16943

Thind, A.K., **Wicker, T.**, **Šimková, H.**, **Fossati, D.**, **Moullet, O.**, **Brabant, C.** ***et al.*** (2017) Rapid cloning of genes in hexaploid wheat using cultivar-specific long-range chromosome assembly. *Nature Biotechnology*, **35**, 793–796. Available from: https://pubmed.ncbi.nlm.nih.gov/28504667/

Tucker, E.B. (1993) Azide treatment enhances cell-to-cell diffusion in staminal hairs of Setcreasea purpurea. *Protoplasma*, **174**, 45–49.

Tyanova, S., **Temu, T.** & **Cox, J.** (2016) The MaxQuant computational platform for mass spectrometry-based shotgun proteomics. *Nature Protocols*, **11**, 2301–2319. Available from: https://pubmed.ncbi.nlm.nih.gov/27809316/

Včelařová, L., **Skalický, V.**, **Chamrád, I.**, **Lenobel, R.**, **Kubeš, M.**, **Pěnčík, A.** ***et al.*** (2021) Auxin metabolome profiling in the Arabidopsis endoplasmic reticulum using an optimised organelle isolation protocol. *International Journal of Molecular Sciences*, **22**, 9370. Available from: https://www.mdpi.com/1422-0067/22/17/9370

Wang, J., **Ma, X.M.**, **Kojima, M.**, **Sakakibara, H.** & **Hou, B.K.** (2013) Glucosyltransferase UGT76C1 finely modulates cytokinin responses via cytokinin N-glucosylation in Arabidopsis thaliana. *Plant Physiology and Biochemistry*, **65**, 9–16. Available from: https://pubmed.ncbi.nlm.nih.gov/23416491/

Werner, T., **Köllmer, I.**, **Bartrina y Manns, I.**, **Holst, K.** & **Schmülling, T.** (2006) New insights into the biology of cytokinin degradation. *Plant Biology (Stuttgart, Germany)*, **8**, 371–381. Available from: https://doi.org/10.1055/s-2006-923928

Wolf, P.G., **Karol, K.G.**, **Mandoli, D.F.**, **Kuehl, J.**, **Arumuganathan, K.**, **Ellis, M.W.** ***et al.*** (2005) The first complete chloroplast genome sequence of a lycophyte, Huperzia lucidula (Lycopodiaceae). *Gene*, **350**, 117–128. Available from: http://linkinghub.elsevier.com/retrieve/pii/S0378111905000375

Wulfetange, K., **Lomin, S.N.**, **Romanov, G.A.**, **Stolz, A.**, **Heyl, A.** & **Schmülling, T.** (2011) The cytokinin receptors of Arabidopsis are located mainly to the endoplasmic reticulum. *Plant Physiology*, **156**, 1808–1818.

Xu, J., **Martien, J.**, **Gilbertson, C.**, **Ma, J.**, **Amador-Noguez, D.** & **Park, J.O.** (2020) Metabolic flux analysis and fluxomics-driven determination of reaction free energy using multiple isotopes. *Current Opinion in Biotechnology*, **64**, 151–160.

Yoo, S.-D., **Cho, Y.-H.** & **Sheen, J.** (2007) Arabidopsis mesophyll protoplasts: a versatile cell system for transient gene expression analysis. *Nature Protocols*, **2**, 1565–1572. Available from: http://www.ncbi.nlm.nih.gov/pubmed/17585298

Zürcher, E. & **Müller, B.** (2016) Cytokinin synthesis, signaling, and function-advances and new insights. In: Jeon, K.W. (Ed.) *International review of cell and molecular biology*. Amsterdam, Netherlands: Academic Press Inc. Elsevier Science, pp. 1–38. Available from: https://doi.org/10.1016/bs.ircmb.2016.01.001

Zürcher, E., **Tavor-Deslex, D.**, **Lituiev, D.**, **Enkerli, K.**, **Tarr, P.T.** & **Müller, B.** (2013) A robust and sensitive synthetic sensor to monitor the transcriptional output of the cytokinin signaling network in planta. *Plant Physiology*, **161**, 1066–1075. Available from: https://pubmed.ncbi.nlm.nih.gov/23355633/